

A Comprehensive Review: Recent Updates on Photocatalytic Degradation of Pollutants Using TiO₂ Photocatalyst

Mehak Nawaz Khan^{1*}, Muhammad Anis Aslam^{1*}, Farhat Bibi¹, Muhammad Sohail Abbas^{2,3*}

¹ Shanghai Key Laboratory of Hydrogen Science & Center of Hydrogen Science, School of Materials Science and Engineering, Shanghai Jiao Tong University, Shanghai 200240, China.

² CAS Key Laboratory of Nanosystems and Hierarchical Fabrication, CAS Center for Excellence in Nanoscience, National Center for Nanoscience and Technology, Beijing 100190, P. R. China.

³ Department of Chemistry, University of Malakand, Chakdara, Dir-L, Pakistan.

Abstract

Environmental sustainability is a challenging task for worldwide researchers. The photocatalyst is a promising technique, which can accomplish this task and resolve the problem in an ecofriendly way. Volatile organic compounds (VOCs) and some inorganic gases are the most hazardous compounds in the environment, which can be abated through photocatalysis. Metal oxide photocatalysts are extensively used for the photocatalytic degradation of VOCs and inorganic gases. Among the metal oxide photocatalysts, Titanium oxide (TiO₂) is the most commonly used semiconductor photocatalyst due to its structure, unique properties under ultra-visible light, nontoxicity, and high acid-base properties, good chemical and thermal stabilities, easy availability, and high metal-support interaction. This review elucidates the morphology, reactive facets, reaction mechanism, structural modifications, surface properties, and key issues related to understanding the importance of TiO₂ as a photocatalyst for the degradation of VOCs and inorganic gaseous pollutants.

Keywords: Titanium oxide; Photocatalysis; Photodegradation; Volatile organic compounds; Catalyst design; Pollution

1. Introduction

Nowadays, the increasing concentration of gaseous organic pollutants is a raising challenge for developing countries and their developing economies and it is the field of interest for many researchers to address the challenges regarding air pollution, toxicity and corresponding mitigation [1, 2]. The degradation of air and water pollution by the solar photocatalytic oxidation approach in the field of interest because it destroys the pollutants completely, while other processes can only separate them. Mostly, volatile organic compounds (VOCs), CO_x , NO_x and SO_x are considered to be responsible for the greenhouse effect; especially, researchers interest increased when they learned to know that acetaldehyde is the major cause of indoor pollution [3-6].

Photocatalysis is the process in which the reaction occurs through the solar & UV energy without using the toxic chemicals and any extra energy. Volatile organic compounds such as acetaldehyde, formaldehyde, and toluene are some important typical organic compounds that are the root of indoor air pollution and are needed to be photo catalytically cleaned to purify the air [2, 7]. These VOCs are emitted from the consumer's goods and construction materials, which not only deteriorate the air quality by forming photochemical smog and atmospheric $\text{PM}_{2.5}$ but they are also carcinogenic and, hence, they cause serious effects to the cardiovascular system [8, 9]. It is reported that the VOCs contents in indoor air is 5-10 times higher than that of outdoor air as estimated by the United States Environmental Protection Agency (U.S.EPA), and currently, it is recommended that about 50% of precedent controlled pollutants are VOCs [10, 11].

Various techniques were applied and studied for the removal of VOCs including biological treatment, physically adsorption, chemically absorption, non-thermal plasma and catalytic combustion [12, 13]. The aforementioned methods have certain limitations, such as high cost and energy consumption, the formation of secondary pollution and the inherent difficulty to deal with low VOC concentration, i.e., to have sufficient conversion [8]. Another

abatement technique is heterogeneous photocatalysis, where Nano semiconductors are used for VOC degradation, using air as oxidant. This process happens under mild conditions at ambient temperature and atmospheric pressure [1, 14].

Transition metal oxides have shown promising properties in catalytic oxidation reactions for the degradation of VOCs [15-17]. Titanium oxide (TiO_2) is one of the most important and active semiconductor photocatalysts having low cost, high chemical stability, nontoxicity, easy availability, high ultraviolet absorptivity, excellent photocatalytic activity, unique physical and electronic properties with larger band gap of 3.2eV [18-21]. TiO_2 under irradiation of UV and near UV light can oxidize VOCs and varied organics into the non-toxic CO_2 , H_2O and mineral acids at ambient temperature and atmospheric pressure [22, 23].

It is widely known that TiO_2 can degrade the pollutants of air and water and that it does not only absorb UV light, but it can also absorb in the visible wavelength area and effectively absorb natural sunlight [24, 25]. As TiO_2 is abundantly used as suspended particles in solution, an effective immobilization of TiO_2 on an adsorbent can largely increase its efficiency to remove pollutants. Since photocatalysis is an emerging technology using TiO_2 as a photocatalyst to oxidize VOCs into CO_2 and H_2O under irradiation of UV light for the purification of indoor air at room temperature and pressure. Currently, the focus of scientists is to enhance the efficiency and selectivity of photocatalysts [26]. The focus of this review is to provide a comprehensive overview of current advances in photocatalytic treatment of gaseous pollutants using TiO_2 as a photocatalyst. After a brief introduction to photocatalysis fundamentals, the TiO_2 photocatalyst, modification, and kinetic analysis are explored mechanistically in terms of organic and inorganic gas phase applications. This review is intended to facilitate as both a solid introduction for newbies to the area and a summary update for professional scholars.

2. Methods for the degradation of gaseous pollutants

Some of the most major anthropogenic pollutants produced in urban and industrial regions are volatile organic compounds (VOCs) [27]. Because they are widespread compounds used as industrial cleaning and degreasing solvents, these VOCs are widely used (and produced by) both industrial and home activities [28]. Cooking and cigarette smoke, building materials, furnishings, dry cleaning agents, paints, glues, cosmetics, fabrics, plastics, polishes, disinfectants, household insecticides, and combustion sources are all sources of VOCs [28, 29]. According to the definition of U.S. EPA, VOCs are volatile nature hydrocarbons at normal indoor conditions of temperature and pressure. According to European Union (EU) VOCs are the volatile compounds having boiling point less than or equal to 250°C at 101.3 kPa vapor pressure. VOCs are naturally produced due to wetlands, oceans, forests, and volcanoes. While some major toxic VOCs are formed due to human activities such as emissions through vehicles, manufacturing industries and petrochemical industries [U.S.EPA, 2012] (Table 1). Usually, when VOC is exposed to NO_x, ozone and other chemicals are formed [30]. The formation of carcinogenic smog on the ground by ozone is a major concern.



Common VOC degradation methods, used in the commercial and industrial sector, are membrane separation, adsorption, liquid absorption, thermal oxidation, bio-filtration and catalytic combustion [31, 32]. New technologies use air or controlled environment chambers for the removal of VOCs. Satisfactory results were not achieved by single based removal system due to the variations and complexity of VOCs characteristics. Therefore, an affective, cost-effective method and environmentally friendly method must be required for the degradation of VOCs. Table 2 provides brief information related to the methods used for the degradation of VOCs [10].

The most traditional technique for the degradation of VOCs is adsorption method. Adsorption techniques required porous materials such as silica gel, activated carbon, and

molecular sieve as a medium for the chemical and physical adsorption. Inorganic salts (e.g., ammonium and sulfurous) along with amine groups such as urea and its derivatives, amino-containing polymers and hydrazine are the commonly used adsorbents [33].

Table 1: Annual concentration limits of air pollutants excluding heavy metals [34].

Pollutants	WHO (mg.m⁻³)	US EPA (mg.m⁻³)	China MEP (residential area) (mg.m⁻³)
PM ₁₀	0.02	N/A	0.04
PM _{2.5}	0.01	0.012	0.04
NO ₂	0.04	0.053	0.04 (24h)
SO ₂	0.02 (24h)	0.5 (3h)	0.02
CO	N/A	N/A	4 (24h)
VOCs	N/A	N/A	Benzopyrene 0.000001

The catalytic oxidation method and thermal process are the most effective techniques for the degradation of VOCs. Reacting formaldehyde with oxygen in the existence of noble metal results in the formation of CO₂ and water [35]. Such reactions occur at high temperatures, so energy consumption is the major issue in such reactions. Particles, atoms, molecules, and free radicals require high chemical activation energy thus it is difficult to control under normal conditions due to the slow reaction rate [10]. Microbial degradation is also a feasible technique used in industries and laboratories for formaldehyde removal from exhaust gas and wastewater. Acidity is the most significant factor in the selection of biological enzymes for degradation. According to experimental data, the removal rate for the enzymes for the degradation of formaldehyde was 80% in 8h. However, these techniques are not applicable to the cleaning of indoor air [36, 37].

Table 2: Summary on current control methods for volatile organic compound degradation [10].

Techniques	By Products	Advantages
Catalytic Combustion	CO ₂ , H ₂ O	Wide range of applications, high efficiency, no secondary pollution.
Activated carbon-based adsorption	Carbon and collected organics	Recovery of compounds, which may offset annual operating costs.
Absorption	Water waste	Product recovery can offset annual operating costs.
Botanical purification	Organics, CO ₂ and amino acids	Economical, no pollution, improving the indoor environment.
Bio filtration	Biomass	Little or no energy needs to be added in the form of heat or radiation to support this process.
Zeolite based adsorption	Zeolite and collected organics	Effective in more than 90% RH as the adsorbent might be too specific.
Membrane separation	Exhausted membrane	The stability of the membrane was poor.

Photocatalytic oxidation (PCO) being a cost-effective, environmentally friendly has received the attention of scientists these days due to its exceptional properties. Removing indoor air VOCs, PCO technology is considered as the most promising technique during recent years. PCO oxidize even low concentrations of VOCs, inorganic, organic nature of gases and convert harmful gases into harmless CO₂ and water [2].

3. General characteristics of Titanium Oxide

Photocatalysts are materials used for degradation of harmful air pollutants into less harmful or harmless form in the presence of UV irradiations [38, 39]. Many scientists have synthesized different photocatalysts for the degradation of VOCs. Various mono component semiconductor photocatalysts e.g., TiO₂ [40-42], ZnO₂ [43, 44], WO₃ [45, 46] and SnO₂ [47, 48] have shown the efficiency for the degradation of VOCs. Photocatalytic oxidation of gas phase VOCs can widely be studied by using TiO₂ as photocatalyst [49, 50]. TiO₂ is a well-known for its easy synthesis, it is well researched, it has photo corrosion resistive, photocatalytic and strong

oxidizing material, and it is mainly used for environmental remediation due to its chemical structure, properties and biocompatibility [51, 52].

3.1 Morphology

The proper applications of TiO_2 depend mainly on the morphology, crystalline polymorphs, and dimensions. In various studies, TiO_2 is prepared to have different forms, shapes, sizes and dimensions like cubes, spheres, tubes, rods, wires, sheets, needles, flakes, flowers, chestnuts, belts, and urchins [19, 53-55]. TiO_2 can exist in three mineral forms i.e., anatase, brookite and rutile (Figure 1)[56-58]. Anatase is the tetragonal crystalline form of TiO_2 and is used as a photocatalyst under UV illumination. Anatase TiO_2 is inexpensive, non-toxic, high surface area, photochemically stable and has a high tendency to generate photoelectrons and have a negative conduction band potential. Anatase can disinfect, purify, and remedy the toxic pollutants in water and air because of its highly photo-induced redox power. Rutile has also a tetragonal crystalline structure and is used in paints with white pigment, whereas brookite has a crystalline orthorhombic form of TiO_2 [56, 59, 60].

In catalytic applications, anatase TiO_2 showed the highest photoreactive activity[61], whereas rutile TiO_2 showed a lesser surface affinity for organic compounds and have high electron-hole recombination rate (Table 3) [62]. It has been investigated that TiO_2 photocatalytic activity is because of its crystalline nature but several authors also reported a controversial result in the literature. Some researchers have reported that the anatase form performs better than the rutile form [63], while others reported the opposite [64]. Some other researchers have noticed and reported that the anatase-rutile hybrid form has best photocatalytic activity [65], but it was recently reported that when the activity of both crystalline forms was compared, the photocatalytic activity depends upon the oxidant composition, e.g., anatase form of TiO_2 showed better photocatalytic activity in the presence of O_2 , while the rutile form of TiO_2 shows highest photocatalytic activity with H_2O_2 [66]. It was

reported that the high photoactivity of anatase was due to the position of the Fermi level, which is higher for anatase than rutile [67].

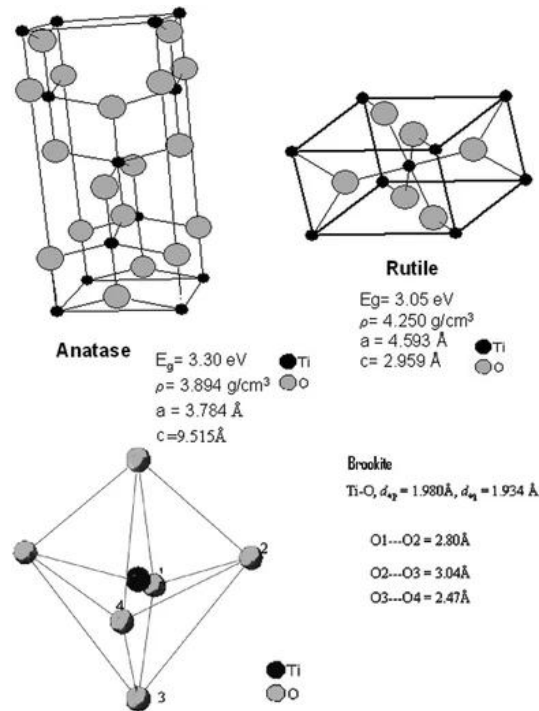


Figure. 1 Different forms of TiO_2 . [58] Copyright 2018 Elsevier.

Table 3. Physical Properties of anatase and rutile forms of TiO_2 [66].

Properties	Anatase TiO_2	Rutile TiO_2
Molecular weight (g/mol)	79.88	79.88
Crystal structure	Tetragonal	Tetragonal
Melting point ($^\circ\text{C}$)	1825	1825
Boiling point ($^\circ\text{C}$)	2500–3000	2500–3000
Light absorption (nm)	<390	<415
Refractive index	2.55	2.75
Ti-O bond length (\AA)	1.95 (4)	1.95 (4)

	1.98 (2)	1.98 (2)
Lattice constant (Å)	a = 4.59	c = 2.96
	a = 4.59	c = 2.96

The physicochemical properties of a catalyst depend upon the preparation method and the used precursors. Degussa P25 TiO₂ is a non-porous 70% anatase –30% rutile compound and it is proven to have higher reactivity than pure anatase and was set as a standard material in the environmental applications of photoreactivity [68]. Hence, the anatase-rutile hybrid form has higher photocatalytic activity, the electrons jump from the conduction band of anatase to the less positive rutile thus recombination rate of electron and hole reduces in the anatase part. The morphology design of the TiO₂-based materials has been synthesized by sol-gel, solvothermal hydrothermal, direct oxidation, micelle and inverse micelle usage, electrodeposition, emulsion or hydrolytic precipitation, chemical/physical vapor deposition, microwave, and ultrasonic techniques [19].

Monodispersed nanoparticles of TiO₂ are the most frequently used morphology due to their small crystalline size and large surface area. The recombination of electrons and holes in bulk is strongly reduced, so that detrimental effects such as surface recombination and low crystallinity due to small size can be avoided [69]. The most preferable titania was synthesized by electrochemical anodization on titanium metal foils using self-assembled nanotubular films where one dimensional (1D) TiO₂ nanotubes, nanowires nanorods, nanoneedles, nanobelts were also synthesized by hydrothermal method. Vectorial charge transfer, controlled porosity [70, 71] and lower recombination rate, enhanced their advantages in photo-induced especially in photocatalysis applications due to their morphology [70-72]. The SEM, TEM, and XRD characterization methods are used for the study of surface morphology and physical properties such as crystalline forms, crystal sizes, facets, and surface area of prepared TiO₂. Nguyen-Phan and Eun Woo Shin [73] reported that by hydrothermal process pure anatase TiO₂ was formed by using a low volume of HCl (DTC-2.15) having quantity >100µm while pure rutile TiO₂ was

prepared by using a high volume of HCl (DTC-15) with spherical morphology (6-8 μm). Changing the volume of HCl from 5-9ml (DTC-5.0, DTC-6.0 and DTC-9.0), the morphology of TiO_2 nanoparticles was changed from a flower-like shape to a cauliflower-like shape where the crystal size became enlarged.

The visible light-responsive TiO_2 can be formed by adding a small quantity of cations and metal oxide by doping and physical ion implantation methods. Visible light-responsive thin film TiO_2 photocatalyst can convert H_2O into pure H_2 and O_2 using sunlight radiations where single site TiO_2 zeolite framework can reduce carbon dioxide and hydrogen into oxygen and hydrocarbons. TiO_2 is among those few materials with photo-induced super hydrophilicity, where photo-functionalized titanium can be used in bone-implant fixation to allow quick bone-titanium integration [26]. Super hydrophilicity and photo-induced redox potential are the two main properties which is the basis of photocatalyst environmental application [19, 25].

3.2 Reactive facets

Spherically shaped TiO_2 has high photocatalytic properties due to its large surface-to-volume ratio and larger number of active sites [74]. The small size of the nanocrystals favors the recombination of electrons and holes having low quantum efficiency and wider band gap, which can deactivate TiO_2 under UVA light [75]. Such complications limit the commercial use of TiO_2 and, hence, modifications to enable UV light absorption will improve electron-hole separation which enhances the corresponding photocatalytic performance. The modification methods like transition metals doping [76, 77], non-metals deposition [78], incorporation of noble metals [79], semiconductor heterojunctions [80], co-catalyst loading and changes of crystal structures were applied to improve the photocatalytic activity of pure TiO_2 (Table 4) [81]. (001), (010) and (101) are the low index fundamental facets of TiO_2 . Morphologically controlled crystal facet structure of anatase TiO_2 and fabrication at the atomic level, i.e., micro and nanoscale level is the topic of scientific research interest these days. According to Wulff

construction [82, 83] anatase TiO_2 is naturally the most dominant with lesser reactivity and thermodynamically stable surface (101), which consist of more than 94% of the surface exposed area. The most commonly and naturally existing shape of TiO_2 is octahedral bipyramid having eight (101) side facets and two top and bottom (001) facets [84]. Meanwhile, the crystal growth during equilibrium the high energy (001) facet disappear and transferred into the specific low surface free energy minimizer shape with bare facets [85-87].

The aspect ratio of the crystal is well-defined as the ratio between the truncation facet sides ((b) and the bipyramidal sides ((a) in Figure 2. The degree of truncation (B/A) ranges from 0.3 to 0.4 with wide range of conditions having less than 10% bare facets (001) [88]. Thus, theoretical and experimental investigation showed that anatase TiO_2 with facets (001) results in a higher catalytic activity, compared to the thermodynamically stable facets (101) due to lower atomic coordination numbers of the bare atoms, active high density unsaturated coordination Ti atoms and surface-active oxygen atoms with broad bond angles of Ti–O–Ti in the facets (001) [89-91]. The modification, applications, and properties of highly energetic (001) facet depends upon the shape of the facets. The reported average surface energy order of the anatase TiO_2 is 0.90 J m^{-2} for (001), $>0.53 \text{ J m}^{-2}$ for (100), and $>0.44 \text{ J m}^{-2}$ for (101) [92, 93]. The low defect TiO_2 nanosheet can decrease the recombination rate of photo generated electrons and holes at the grain boundaries and attain the high energy conversion efficiency. By doping anatase TiO_2 nanosheets with bare energetic facets (001) with metals and non-metals, the absorption of UV light enhanced. Carbon [94], nitrogen, sulfur [92, 95] nickel [96], molybdenum [97], platinum [98] and aurum [99] are the metals used to dope the faceted TiO_2 . Many novel forms of the anatase TiO_2 (001) facet received much attention of the researchers from the past few years and published different reviews on the pure anatase TiO_2 facet (001) [100, 101].

Table 4. Photocatalytic oxidations of volatile organic compounds on TiO₂-based photocatalyst [34].

Photocatalyst	Pollutants	Performance	Reference
Silica glass fibers doped P25 Degussa TiO ₂	Acetylene	85% acetylene was degraded with the formation of formaldehyde, formic acid and glyoxal as intermediates	[102]
A monolithic catalytic bed coated with P25 and PC500	n-decane and perchloroethylene (PCE)	n-decane decomposition rate was 100% where PCE was degraded by 69%	[103]
Graphene oxide on TiO ₂ nanocrystals	Benzene and ethanol	95% conversion	[104]
PVC sheet coated by TiO ₂	Toluene and benzene	Rate constant of 7.65 x 10 ⁻⁵ and 1.07 x 10 ⁻⁴ min ⁻¹ /cm ²	[105]
Optical fiber coated by TiO ₂	Isopropanol	22% conversion	[106]
TiO ₂ film on window glass	Benzene and acetone	100% Benzene and acetone was degraded in 25 min and 110 min	[107]
TiO ₂ film mechanically robust	Acetaldehyde and ethanol	Under UV 100% conversion in 70 min for ethanol and 125 min for acetaldehyde	[108]
Nano and micro- sized TiO ₂	Acetaldehyde, toluene and Acetone	PC105 (Cristal) > P25 (Evonik) > 1077 (Kronos) > AT-1 (Cristal)	[109]
TiO ₂ microfiber	Heptane, toluene and acetone	Quantum efficiencies on TiO ₂ fiber for acetone 0.0106, heptane 0.0027 and toluene 0.0024	[110]
Mesoporous TiO ₂	Benzene	80% conversion on TS-400	[111]
F-doped anatase TiO ₂ nanosheets	Acetone, benzene and toluene	Highly efficient under both UV and visible light	[112]
Nanocomposites of TiO ₂ /SiO ₂	Benzene	92.3% conversion for Ti/Si = 30: 1 in 2 h, conversion rate is 6.8 times higher than P25	[113]
TiO ₂ doped with Fe ₂ O ₃	Trichloroethylene (TCE)	95% degradation of TCE	[114]
TiO ₂ doped with transition	Benzene	58% conversion by Mn/TiO ₂	[115]

metal TiO ₂ doped by Cu		TCE	Both TCE and water mobility was favored by 0.2 wt% Cu content where 0.5 wt% Cu blocked the active sites strongly	[116]
V-doped polyurethane	TiO ₂ /porous	Toluene	80% degradation	[8]
Sn ²⁺ -doped TiO ₂		Benzene	27% conversion by TS-40 (Ti/Sn = 40: 1)	[117]
TiO ₂ doped with Pt		Cyclohexane	100% decomposition and platinum endorsed the CO ₂ selectivity	[118]
N-doped and O-deficient TiO ₂		N-doped Benzene	72% benzene converted and yields CO ₂ of 190ppmv for 5 h reaction	[119]
Spray-coated polyester fiber supported non- metal doped TiO ₂		Formaldehyde	38% conversion at C-TiO ₂	[120]

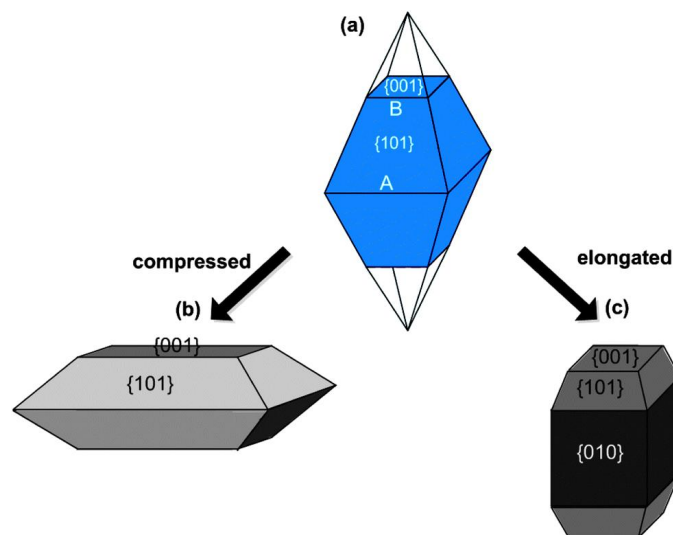


Figure 2: Evolution of an anatase TiO₂ crystal nucleus nucleated as a truncated octahedral bipyramid seed: (a) under equilibrium conditions, the high energy (001) facets diminish rapidly, and the crystal evolves into thermodynamically stable (101) facets. (b and c). Under non-equilibrium conditions, the high energy (001) and (010) facets are stabilized by selective adhesion of capping agents. The side lengths labelled as (A) and (B) are used to estimate the

degree of truncation (B/A) and calculate the percentage of exposed (001) facets [121].
Copyright 2014 Royal Society of Chemistry.

3.3 Engineering of oxygen vacancies

Oxygen vacancies in photocatalytic reactions play an important role and get the attention of scientists to engineers. TiO_2 is the most used semiconductor oxide for the degradation of environmental pollution and the generation of hydrogen gas photo-catalytically. Reduction of electron-hole recombination and the introduction of oxygen defects are the most promising ways to enhance photocatalytic activity [122, 123]. Surface oxygen vacancies can trap the photoinduced charge and subsequently provide sites for the adsorbed compounds by transferring the charge which inhibits the recombination of the charges, leading to an increase in photocatalytic activity. Oxygen vacancies in the bulk play an important role as charge trappers and decrease the photocatalytic performance due to the recombination of photo-generated electrons and holes [124-126]. However, it is important to control the surface oxygen vacancies to increase the performance of the photocatalyst. The disordered layer was formed by Mao et al. in TiO_2 by hydrogenation method which improved the photocatalytic performance of TiO_2 [127]. Surface oxygen vacancies of TiO_2 get more attention than bulk oxygen vacancies. Two different types of intrinsic defects (surface oxygen vacancy $V_{\text{O}}^{\bullet\bullet}$ and TiO^{3+}) are formed on the surface of TiO_2 simultaneously when reacting with hydrogen or any other reducing agent at high temperature [128]. The simplest and widely studied method for the generation of surface vacancy is to treat the nanocrystals of TiO_2 by hydrogen thermal method [127, 129, 130]. Surface vacancy/reduced TiO_2 nanomaterials with different shapes, sizes and morphology are also formed by chemical reduction or oxidation and electrochemical reduction method with $V_{\text{O}}^{\bullet\bullet}$ [129, 131-133].

A literature study showed that both surface and bulk oxygen vacancy increases light absorption, but they have different effects on photocatalytic activity. The oxygen vacancy

defects in TiO_2 were theoretically studied by first-principles calculations [134, 135], electron paramagnetic resonance spectroscopy (EPR), scanning tunnelling microscopy (STM) [136-140] and time-resolved photoluminescence spectroscopy (PL) [125, 127] are the experimental techniques used for the study of oxygen vacancy defect in TiO_2 . These defects may also affect the electronic properties [141], reactivity, adsorption and desorption of anatase and rutile with O_2 [135-139], H_2O and CO_2 has been reported. Li et al. [142] investigated that the oxygen vacancy defect level is situated below the conduction band in TiO_2 . Studies have been reported that the free electrons on oxygen vacancy are localized to form Ti^{3+} center [143]. The TiO_{2-x} contained oxygen vacancy under visible light showed enhanced photocatalytic activity [127, 144]. Due to the defects caused by oxygen vacancy, visible light absorption increased in TiO_2 , where the catalytic activity was improved due to the absorption of solar light. Fukushi et al. [145] reported the results contrary to the above with the reduction of photocatalytic activity under fluorescence lamp for the degradation of organic materials in gas phase. This result was due to the different illuminating material used. For defect less TiO_2 UV light can be used, whereas for defected TiO_2 visible light is effective. Due to the presence of oxygen vacancies, free electrons can move between the surface and the bulk and, hence, more electrons were absorbed by the holes after light incidence [146-148]. The above literature studies reveal that the holes, affecting the degradation of organic materials, decreased and, as consequence, this corresponded to an enhanced photocatalytic activity.

Li et al. [149] explored the three different kinds of TiO_2 nanocrystals for the photocatalytic reduction of CO_2 by two different vacancy defects: the surface oxygen vacancy (SO) and bulk single-electron-trapped oxygen vacancy (SETOV). The former was prepared by the reduction of anatase TiO_2 (SO- TiO_2) using NaBH_4 . Nanotubes titanate were dehydrated to form bulk-SETOV (SETOV-BO) at 400°C whereby reducing pristine TiO_2 the surface and bulk oxygen vacancy (SBO) were produced at high temperatures. After investigation the high photocatalytic reduction was shown by the photocatalyst with both surface and bulk defects and the increase of the surface defects over the bulk enhanced the photoreduction of CO_2 as

shown in Figure 3. Huang et al. [150] reported that a CuO_2 ultrathin layer on TiO_2 nanorods surface was formed by the redox reaction between Ti^{3+} induced by oxygen vacancy and Cu^{2+} . The oxygen vacancy modulation defect could obviously increase the efficiency of anatase/brookite heterophase junction 12 times higher than pristine TiO_2 [151].

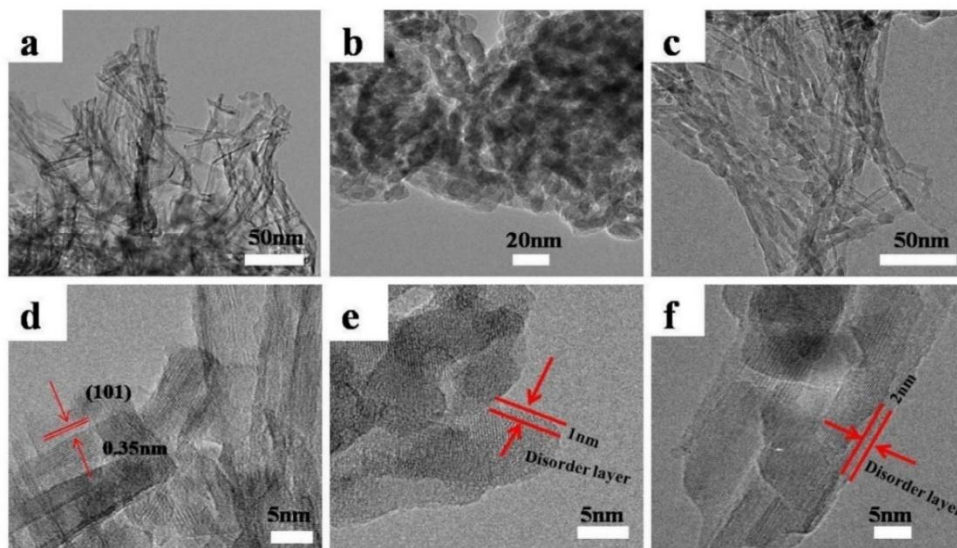
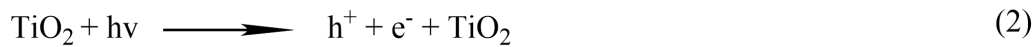


Figure 3: TEM and HRTEM images of $\text{TiO}_2\text{-BO}$ (a, d), $\text{TiO}_2\text{-SO}$ (b, e), and $\text{TiO}_2\text{-SBO}$ (c, f) [149]. Copyright 2017 Elsevier.

4. Reaction mechanism of TiO_2 photocatalyst

Mechanism of photocatalytic oxidation reactions (PCO) have key importance in the real applications. During the PCO, the formation of electron and hole between the valance (VB) and conduction band (CB), is the significant step and needs energy to overcome the band gap energy (E_g) [56]. The oxidation and reduction process can occur at the same time in PCO reactions. The free photoelectron in the CB and a photohole in the VB are created in the semiconductor by the absorption of photon of energy equal or greater than the energy

difference between the VB and CB. The photo-redox reaction occurs between the air, pollutant and oxygen simultaneously. The hydroxide (HO^-) or hydroxyl radical (HO^\bullet) formed during the PCO reaction is very reactive while the superoxide (O_2^-) formed by reducing oxygen (O_2) as a result of the electron reducing ability [66]. The organic or inorganic pollutants and microorganisms can be destroyed by the highly reactive HO^\bullet and O_2^- species (Figure 4) [152-154]. TiO_2 has the ability for the complete degradation of organic pollutants, and the activation can be expressed by Equation (2) [66]:



The photonic excitation in the above reaction is the initiating step for the catalytic reaction, where h^+ and e^- are the strong oxidizing and reducing agents correspondingly:



The reduction reaction:



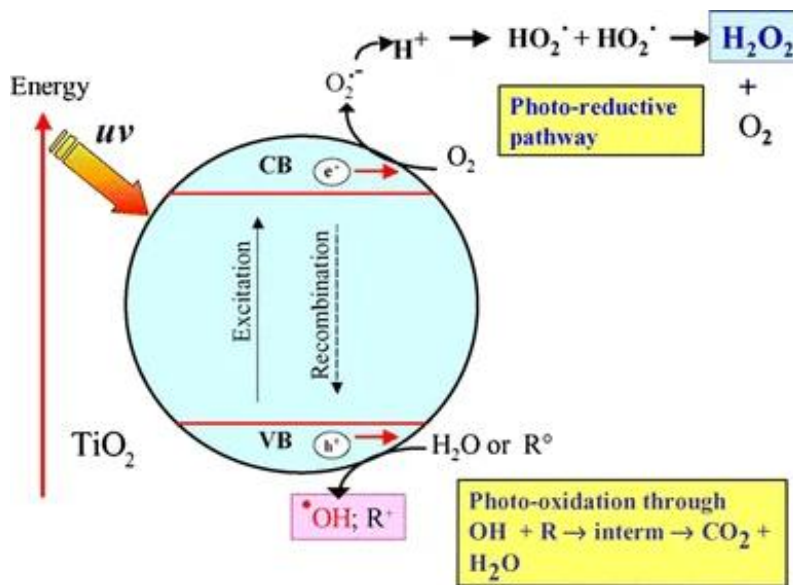


Figure 4: Classical scheme for the production of highly oxidative species by TiO₂ under light irradiation with wavelengths <400 nm. [56] Copyright 2011 Springer.

5. Photocatalytic degradation of organic gaseous pollutants

In the early 1970's gas-phase heterogeneous catalysis was examined by Teichner et al. [155] for the incomplete oxidation of paraffins and photocatalytic oxidation of isopropanol and photo-adsorption of oxygen and the formation of reactive species after the adsorption of water on the surface of TiO₂ were studied by Stone et al. on rutile surface [156, 157]. Firstly, surface OH_s⁻ and bulk OH_L⁻ were reported to be formed on the surface of Ti⁴⁺O₂²⁻. On the reactive surface of TiO₂, the positive hole was trapped by OH⁻ to form •OH while O_{2, ads} after getting electron produced O_{2, ads}^{•-}. The reactive radicals, present in the photodegradation process, are produced during water and oxygen adsorption at the surface and are capable of the degradation of VOCs in the air by PCO reaction [157]. Further studies of chemisorption and photochemistry of CO₂, O₂, and H₂O can provide concepts about the degradation of VOCs in the air purified by PCO (Figure 5). The World's attention is attracted by indoor air pollution for the PCO of VOCs due to

its health effect [34]. Indoor and outdoor air pollutants mainly consist of VOCs i.e., aldehydes, aromatics, and halocarbons. Benzene, toluene, formaldehyde and tetrachloroethene are the frequently used VOCs in PCO studies used for the better understanding of the photocatalysts and reactors.

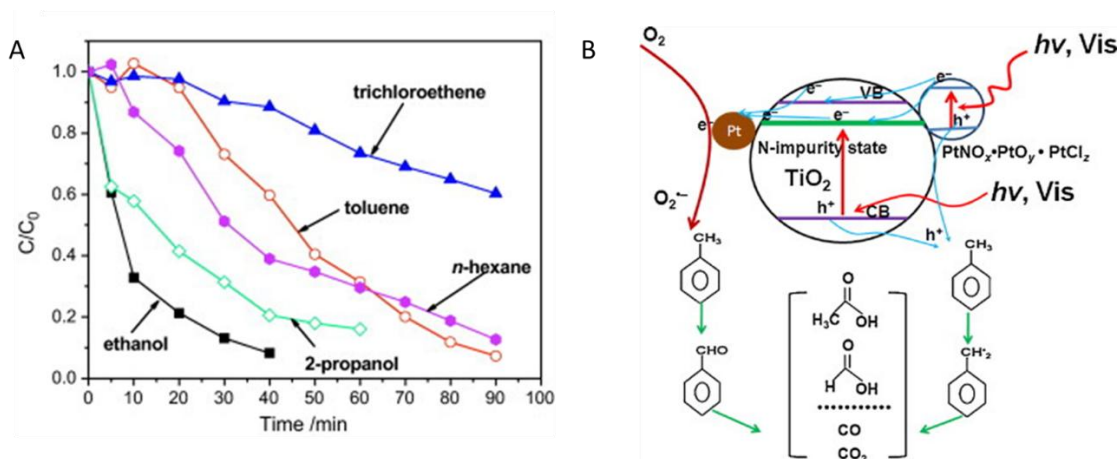


Figure 5: (A) Degradation of various chemicals using Pt/N-TiO₂ photocatalyst. (B) Mechanism of photodegradation of gaseous toluene over Pt/N-TiO₂ under visible light irradiations. [158] Copyright 2011 Elsevier.

5.1 Photocatalytic Degradation of Aldehydes

Environmental pollution due to aldehydes is the main concern of scientists these days. Formaldehyde is the most important air pollutant among carbonyl compounds that causes serious sickness and cancer [159]. The World Health Organization (WHO) limit for formaldehyde in air is 80ppb or 0.1mgm⁻³ [66]. Peral and Ollis [160] were the first to study the heterogeneous photocatalytic oxidation of various pollutant gases e.g., formaldehyde and butyraldehyde as well as m-xylene, acetone and 1-butanol. Gas phase photocatalytic degradation of these compounds was studied by the Langmuir-Hinshelwood rate forms by using anatase TiO₂ powder under UV radiation [161].

Yuanwei Luet al. [22] investigated the adsorption of formaldehyde on the TiO₂ film coated on activated carbon filters and TiO₂ film coated on glass under UV irradiation. TiO₂ coated with activated carbon filters can work efficiently as compared to TiO₂ film coated on glass. Activated carbon-coated TiO₂ significantly increased the degradation of formaldehyde, due to the absence of adsorption saturation over the activated carbon. Elfallah et al.[162] reported the TiO₂-impregnated polyester (PES) and glass fibre (GFT)-TiO₂ for the photocatalytic degradation of butyraldehyde and isovaleraldehyde. GFT-TiO₂ has enhanced the performance as compared to PES-TiO₂. The by-products formed during the reaction were analyzed by gas chromatography-mass spectrometry (GC-MS). Shi and coworkers [163] studied the photocatalytic oxidative conversion of aldehydes into carboxylates using TiO₂ as a catalyst by the oxygen isotope labelling method. The dehydrogenation of aldehydes takes place first, followed by the oxidation of aldehydes by a two-electron transfer process. The photocatalytic oxidation is initiated by •OH and SO• single electron radicals. DFT studies defined a new way for the oxidation of aldehydes using TiO₂ as a catalyst. The aromatic aldehydes (benzaldehyde and p-methoxybenzaldehyde) showed much lower photodegradation performance and yield as compared to aliphatic aldehydes (acetaldehyde and propionaldehyde) as shown in Figure 6. The first order rate constant for p-methoxybenzaldehyde was $2.34 \times 10^{-4} \text{ min}^{-1}$, $3.09 \times 10^{-4} \text{ min}^{-1}$ for benzaldehyde, $27.1 \times 10^{-4} \text{ min}^{-1}$ for propionaldehyde and $30.4 \times 10^{-4} \text{ min}^{-1}$ for acetaldehyde, respectively.

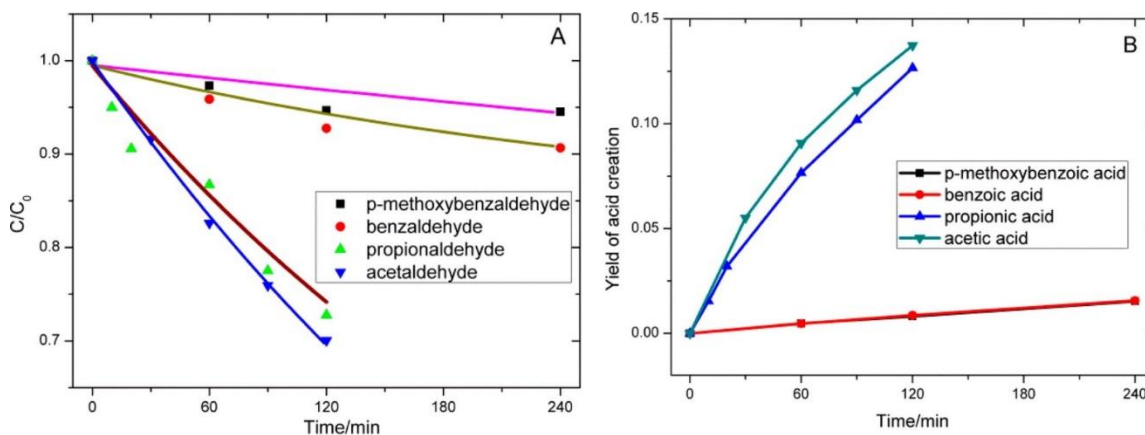
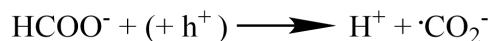
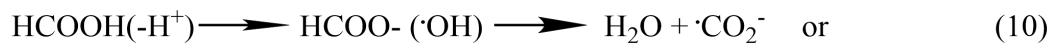
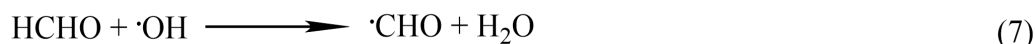


Figure 6. (A) Degradation kinetics of p-methoxybenzaldehyde, propionaldehyde, benzaldehyde, and acetaldehyde and (B) yield of corresponding acids: concentration ratio of the formed acids to the initial aldehydes [163]. Copyright 2015 American Chemical Society.

The proposed mechanism for the photodegradation of formaldehyde is given by Equation (7-11) [34, 164]:



5.2 Photocatalytic degradation of toluene

Toluene is a pollutant, occurring in both indoor and outdoor environments, and it is the most well-known and recommended pollutant by the French normalization group in the standard AFNOR, XP-B44-013 for the study of PCO was prepared the surfaces of TiO₂ nanoparticles by loading TiO₂ quantum dots (QDs) with a two-step method [163, 165]

Quici et al.[166] reported the effect of low concentration of toluene under UV light of 254 nm and 185 nm for indoor air purification using two different forms of TiO₂, one coated with P25 aqueous suspension and the other with thin films organic/inorganic sol gel mesoporous anatase. The efficiency for the removal of toluene was enhanced by increasing the thickness (i.e., mass) of the TiO₂ till 500 nm, while further increase in thickness could not enhanced the removal efficiency. Zhong et al [167] studied removal of toluene using co-alloyed

TiNbON under visible light with radiance 42-95W/m² at room temperature with a relative humidity of 25-65% and flow rate of 0.78cm/s to 7.84cm/s. Visible light can degrade the 58% of toluene. Seunghyun et al. investigated the degradation of toluene using Pt/TiO₂ and F-TiO₂ as a photocatalysts. The Pt/TiO₂ exhibits a greater photodegradation activity as compared to pristine TiO₂, but it rapidly deactivates when repeatedly used. On the other hand, F-TiO₂ initially showed less photodegradation activity, but only a slight deactivation was observed after several runs. The Pt/TiO₂ catalyst showed higher photodegradation activity for toluene (Figure 7).

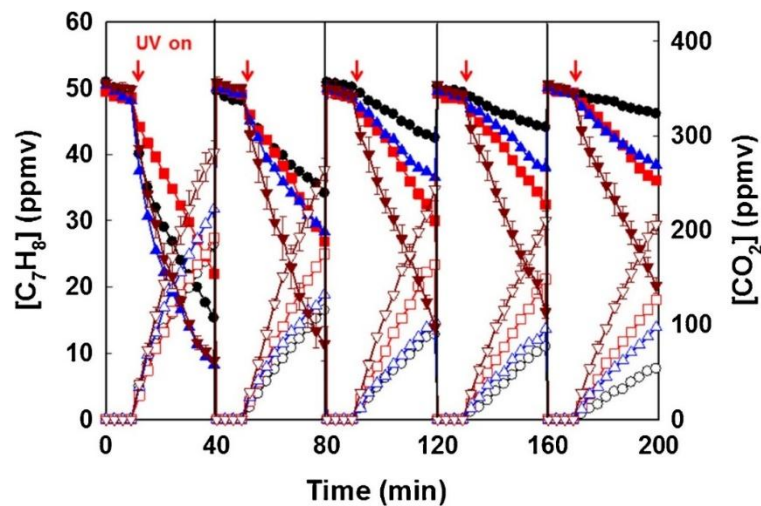
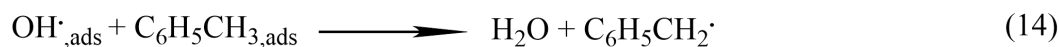
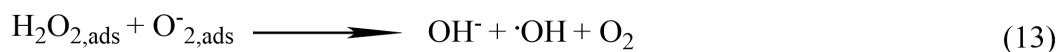
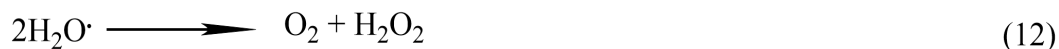
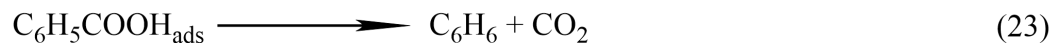
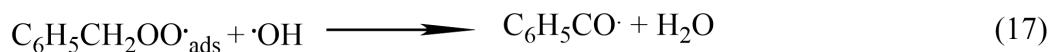


Figure 7. Repeated photocatalytic degradation cycles of gaseous toluene on F-TiO₂/Pt (▼), Pt/TiO₂ (▲), F-TiO₂ (■), and bare TiO₂ (●)[168]. Copyright 2018 Elsevier.

The mechanism for the PCO of toluene gasses provided in (Eq.12-23) [34],





According to the proposed mechanism, benzoic acid and small amount of benzyl alcohol, phenol and benzaldehyde will be produced as intermediates, due to partial oxidation during the degradation of toluene.

5.3 Photocatalytic degradation of Benzene

Chemical factories produce fuel gas, gasoline vapours, automobiles, cigarette smoke, plastics, rubber, and paints are the sources of benzene production, as well as benzene derivatives, such as toluene, benzoic acid, chlorobenzene, phenols and chlorophenols. Health problems like leukaemia due to even a small amount of benzene are reported [169].

To perform PCO of gaseous benzene, Wang and Ku [168] used a batch-type photoreactor with a bundle of TiO₂-coated quartz fibre. The principal intermediate was suggested to be phenol; however, the final products were CO₂, CO, and H₂O. The degradation routes were seen using gas chromatography-mass spectrometry (GC-MS) and Fourier transform infrared spectroscopy, as shown in Scheme 1. Jian et al. [12] prepared mesoporous TiO₂ photocatalyst by changing the calcination temperature for the removal of benzene (Figure 8). Mesoporous TiO₂ shows more catalytic activity and stability as compared to commercial TiO₂ for the degradation of benzene. Yanhui et al. [20] reported that the graphene-TiO₂ has higher

stability and photocatalytic activity towards gaseous benzene, the higher the content of graphene. TiO₂ lower its photocatalytic activity.

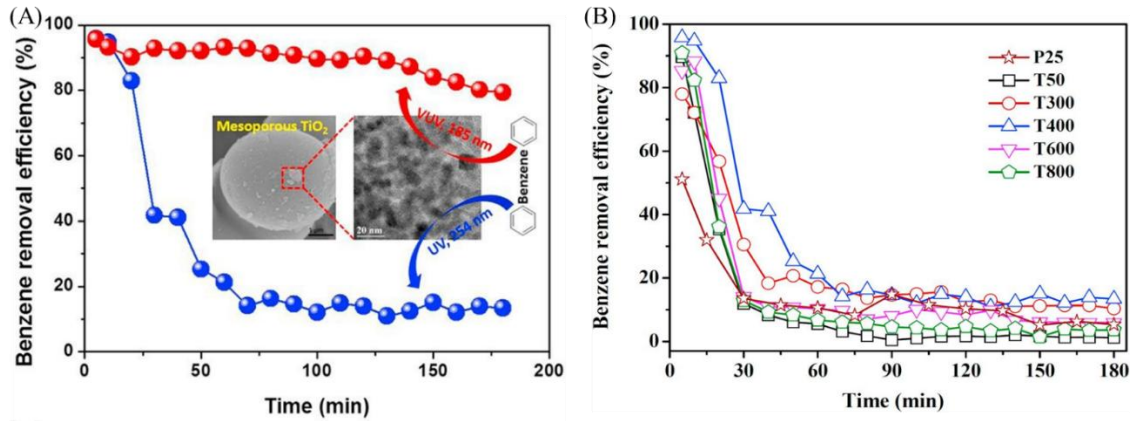


Figure 8: (A) Photodegradation of benzene using mesoporous TiO₂ under UV and VUV irradiation. (B) Benzene removal efficiency over TiO₂ calcined at different temperatures under UV-PCO system [12]. Copyright 2017 Elsevier.

The organochloride compound trichloroethene (TCE) is used as a solvent, cleaning and degreasing agent. TCE is the typical chlorinated VOC emitted from industrial wastes, indoor air and hazardous waste sites [171]. Tomoaki et al [172] investigated the porous Pt ion doped TiO₂ under visible light for the photocatalytic degradation of TCE, which was 100% degraded under visible light (Figure 9).

Being a chlorinated compound, TCE was studied as an air pollutant in PCO. It was observed that the most hazardous and toxic chlorinated VOCs intermediates are formed i.e., carbon monoxide (CO), chloroform (CHCl₃), carbon tetrachloride (CCl₄), dichloroacetyl chloride (DCAC), tri-chloroacetylene chloride (TCAC) and phosgene (COCl₂) during PCO degradation reaction of TCE. The proposed TCE mechanism is given in the scheme given below. It was observed that the toxic effect of intermediates is reduced due to oxygen and relative [90-92]. The effects of oxygen and relative humidity (RH) on the formation of DCAC and phosgene were examined by Ou and Lo [171]. As shown in Scheme 2 [171], a TCE degradation process has been proposed. The number of hazardous intermediates can be reduced by optimizing oxygen and relative humidity.

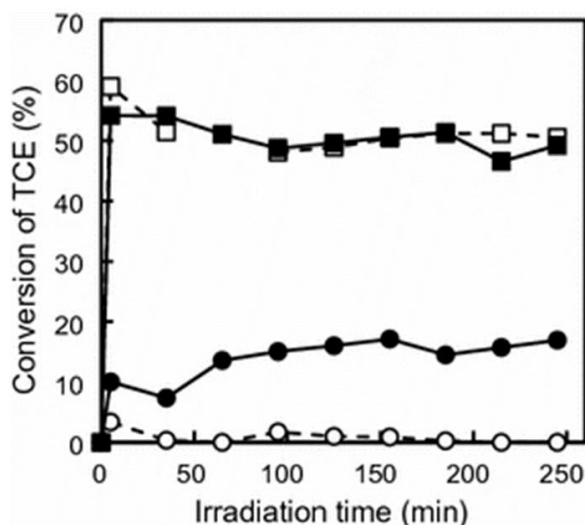
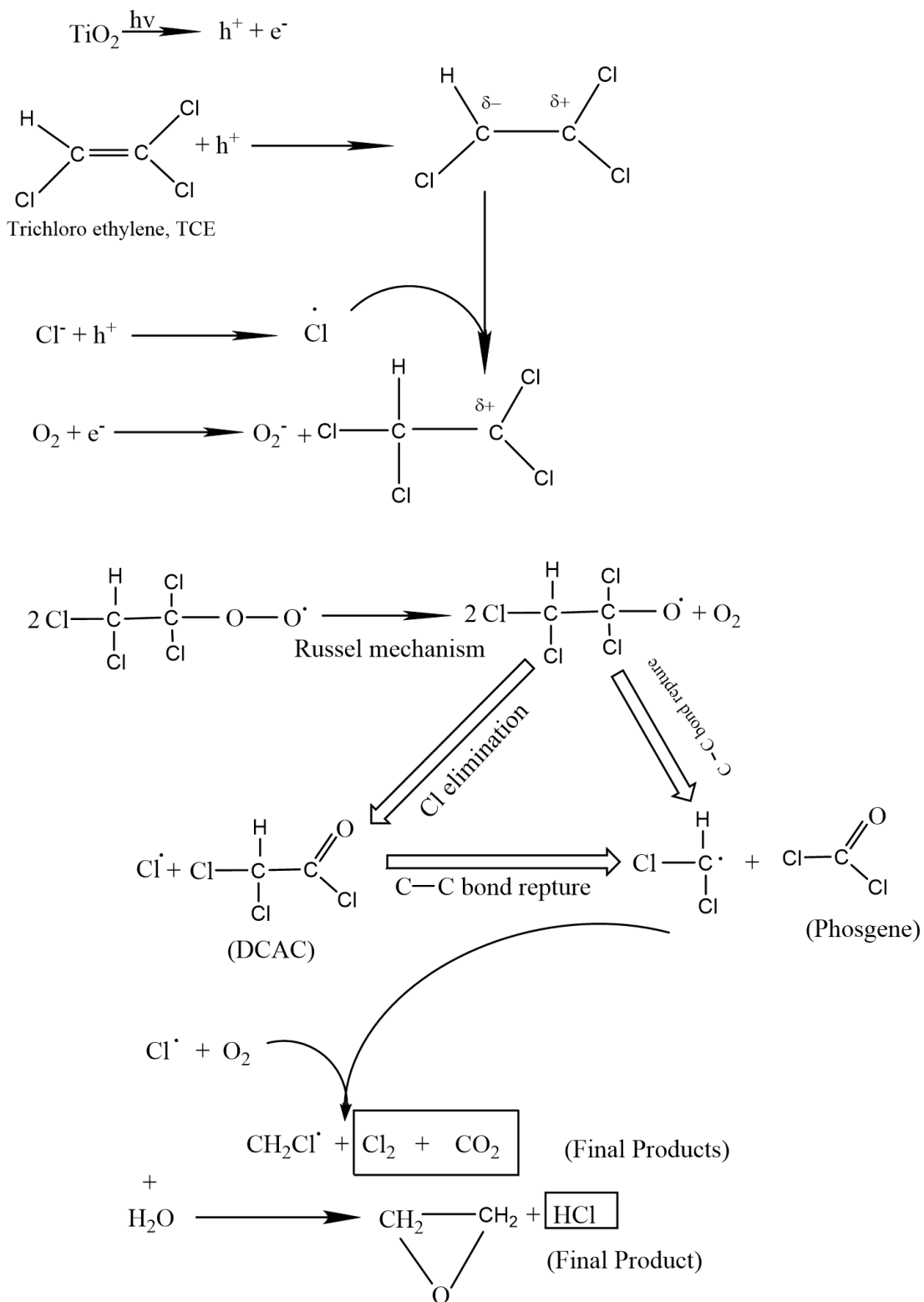


Figure 9: Time course of TCE conversion on Pt-TiO₂(filled circle) and TiO₂(open circle) under VL irradiation and Pt-TiO₂(filled square) and TiO₂ (open square) under UV irradiation [172].
Copyright 2017 Springer.



Scheme 2: Proposed mechanism of TCE photodegradation [173].

6. Photocatalytic degradation of inorganic gaseous pollutants

The massive intrusion of harmful contaminants into environmental matrices is a global threat that is becoming increasingly alarming due to the increase in industrialization. Besides organic pollutants, every year a considerable number of different types of harmful inorganic pollutants, such as NO_x , SO_x , CO , and others, are released. TiO_2 -based photocatalysts are widely used for the photodegradation of these inorganic pollutants (Table 5).

Table 5. Photocatalytic oxidations of inorganic gas pollutants on TiO_2 -based photocatalysts [34].

Photocatalyst	Pollutants	Performance	Reference
Polymeric nanofibers supported anatase TiO_2	NO_x	16% of NO decomposed	[174]
Oxygen-deficient TiO_2	NO	75% of NO degraded	[175]
Fe/ TiO_2	NO_x	38% of NO decomposed	[176]
Molybdenum-doped TiO_2 nanotubes	NO_2	77% decomposition of NO_x	[177]
Pt-doped TiO_2	NO_x	Pt- TiO_2 0.4% decomposed about 30% NO while P25 5% under the irradiations of visible light	[178]

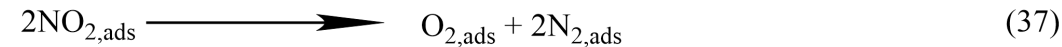
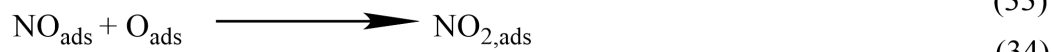
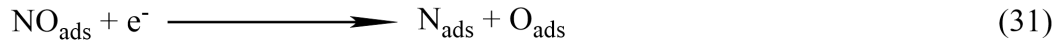
Au/CeO ₂ -TiO ₂	NO	83% of NO decomposition where 48% over	[179]
Cobalt imidazole complex functionalized GO supported TiO ₂ film	NO _x and CO	pure TiO ₂ 51% of NO _x decomposition and 46% of CO greater than pure TiO ₂ film	[180]
WO ₃ /TiO ₂	H ₂ S	70% decomposition of H ₂ S and 60% sulfur was removed	[181]
RuO ₂ /TiO ₂ /Pt	CO SO ₂ and	by 5%WO ₃ /TiO ₂ 100% degradation of CO in 60 min	[182]
Multi-walled carbon nanotubes supported Cu/TiO ₂	NO	62% SO ₂ and 43% NO	[183]
Dye-modified TiO ₂	NO	was removed	[184]
		99% of NO decomposed with 99% N ₂ selectivity	

6.1 Photocatalytic degradation of NO_x

The nitric oxides (NO_x) mainly include NO and NO₂ [185]. Emission of NO₂ may occur due to the activities of both human beings and natural sources, e.g., volcanic emissions, and NO_x and can be emitted by the decomposition of organic compounds by the microorganisms by solar energy and the ecosystem. Human activities and automobiles can emit NO_x. Emission of NO_x can cause human health problems like immune and respiratory problems and environmental issues e.g., global warming, formation of tropospheric ozone and acid rain [186]. The removal of NO_x can be done by controlling NO_x emission by reducing NO_x into N₂ or

oxidizing it into HNO_3 [185, 187]. NO_x can be reduced by heterogeneous photocatalytic oxidation (PCO), HCs-SCR, NH_3 -SCR, photoselective catalytic reduction (photo-SCR) and photodecomposition [5, 111, 188].

Luevano-Hipolito et al. [189, 190] studied the photocatalytic degradation of NO and their $\text{Bi}_2\text{Mo}_3\text{O}_{12}$ catalyst was reported to remove 88.9% NO and is considered to be an excellent photocatalyst under UVA PCO. The TiO_2/WO_3 was studied for nitrogen oxide (NO_x) removal under UV and visible light. Mendoza et al. [191] examined surface-modified WO_3/TiO_2 for NO_x removal under visible light. Host TiO_2 was modified by using NaOH as a modifying agent. The performance of NaOH-modified WO_3/TiO_2 was increased by increasing the concentration of NaOH which can remove more than 90% of NO_x while non-modified WO_3/TiO_2 can remove ~ 72% of NO_x . The greater proficiency for the removal of NO_x was due to the oxygen vacancies on the surface of TiO_2 which facilitates WO_3 particles to bind efficiently. Ma et al. [192] prepared oxygen-deficient TiO_2 (TiO_2 -200) at low temperatures for the degradation of NO at the level of 400 ppbv under visible light irradiations ($420 \text{ nm} < \lambda < 700 \text{ nm}$). Visible light irradiations can be absorbed efficiently due to oxygen vacancies on TiO_2 surface which facilitates the separation of photoelectrons and holes. Larger the surface area larger are the active sites for reaction. The enhanced photocatalytic oxidation ability of TiO_2 -200 is due to oxidation of NO to NO^{-3} as shown in Figure 10. Marco et. al. discusses the production and characterization of sodium titanates (ST) as well as their application in the photocatalytic reduction of NO. The photocatalytic studies revealed that virgin ST (tri and hexa-titanate) was the photocatalyst with the best performance in terms of NO reduction when compared to the impregnated samples (STAg, ST-Zn). When 1 g of photocatalyst was used with a flow of 280 ml/min and a light of 253 nm, maximum degradation efficiencies of 80 percent were achieved [193].

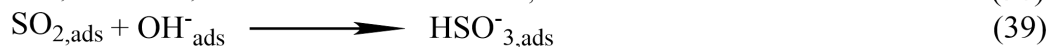
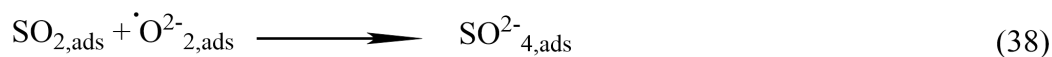


6.2 Photocatalytic degradation of SO_x

The US EPA declared gaseous SO_x as a hazardous pollutant because it can cause damage to the vegetation, acid rain and corrosion to the buildings. Exposure to SO_x can cause respiratory problems like asthma and bronchi tightening. SO_x can also form airborne particles which create problems in visibility and change the climate.

Wang et al. [194] studied photochemical removal of SO₂ over TiO₂-based nanofibers with a dry photocatalytic oxidation process. Results revealed that the degradation of SO₂ under UV light was mainly influenced by the oxidation of NO to NO₂. The researchers found that adding TiO₂ to mortars increased their physical, mechanical, and photocatalytic capabilities, as well as allowing them to be decontaminated by the SO₂ pollutant [195]. Cerium-based TiO₂ nanofibers showed 100% efficiency for the removal of SO₂ and are resistive to humidity while using copper-based TiO₂ nanofibers the photocatalytic activity decreased when humidity is less than 4% where SO₂ dissolution occurs under 8% humidity (Figure 11).

Topalian et al. [196] investigate the photo fixation of SO_x on the surface of anatase TiO₂. Studies have shown active oxygen can facilitate the sulfides and sulfates formed by the photooxidation of SO₂.



Xia et al. [197] described their investigations on the photocatalytic evacuation of vaporous NO and SO₂ utilizing BiOI/Al₂O₃ as a photocatalyst under visible irradiations. The proposed mechanism and the conversion of SO₂ is given below (Equations 40-42),

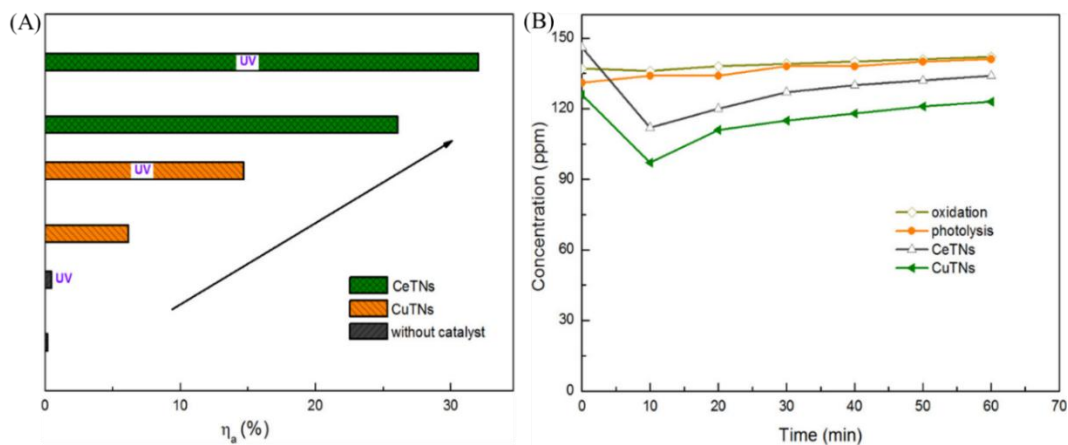
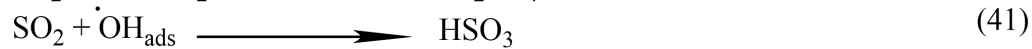


Figure 11: (A) Characteristics of SO₂ photocatalytic removal process. (B) Photocatalytic removal of SO₂ under basic fuel gas (BFG) atmospheres [194]. Copyright 2017 American Chemical Society.

6.3 Photocatalytic Degradation of CO and Ozone

The carbon monoxide is a major air pollutant in the environment and fatal for living beings because it can accumulate oxygen in the blood. CO is emitted by the partial combustion/oxidation of volatile organic compounds, i.e., hydrocarbons. Hassan et al. [198] reported a Ti-MCM-41 mesoporous framework which hindered the crystal growth of TiO₂. This

property can make Ti-MCM-41 more favorable for the photocatalytic degradation of methylene blue and carbon monoxide (Figure 12).

Ozone is a pungent smell blue colour gas located in the atmosphere above 30,000-150,000 feet and is responsible for the absorption of UV rays and protecting the earth from the harmful effects of UV rays. Ozone is a hazardous pollutant and varies with region, temperature and weather. Ozone concentration higher than 0.214g/m^3 is poisonous and can cause headaches, eye, nose and throat irritation and chest pain [199]. Ozone has a strong oxidizing property and oxidizes VOCs in the atmosphere. Simultaneous degradation of pollutants is a topic of interest in this field.

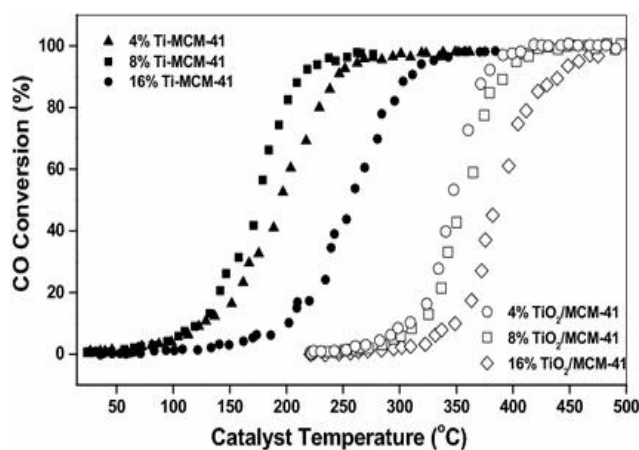


Figure 12: CO conversion % in relation to the reaction temperature over $\text{TiO}_2/\text{MCM-41}$ prepared by post impregnation and Ti-MCM-41 prepared by one pot method containing different TiO_2 content (4,8 and 16 wt%) using gas mixture CO and O_2 with amount (4:20 wt% respectively) at a rate of 100 mL min^{-1} [198]. Copyright 2017 Springer.

Carbon monoxide under UV irradiations converts to CO_2 which is the last step in the photooxidation/ photodegradation of CO (Equations 43-46) [200]:



Ozone can be photo-catalytically degraded due to the formation of reactive radical. Following is the pathway used for the photodegradation of ozone (Equations 43-49),



Other reported pathway for the photodegradation ozone are as follow(Equations 50,51) [199],



6.4 Photocatalytic degradation of H₂S

H₂S is a highly poisonous, odorous, and corrosive gas and is responsible for odour pollution which can affect human health and the environment. H₂S in the range of 0.0004 ppm can cause H₂S corrosion, acid rain and global warming.

Gaoyuan et al [201] described the degradation of H₂S over transition metals (Mn, Cu, Ni and Co) modified TiO₂ prepared by sol gelatin method under VUV-PCO and UV-PCO. Among all the Mn-TiO₂ showed the highest activity for the degradation of H₂S under VUV-PCO. Haiboet al. [202] investigated the hollow double organic metal framework [MIL-101(Cr)] of TiO₂

nanoparticles [TiO₂@MIL-101(Cr)] having high adsorption capability for H₂S under UV irradiations (Figure 13). Naeem et al. [203] reported the comparative studies of photocatalytic degradation of H₂S on the pure and 2% S-doped TiO₂ nanoparticles and nanofibers. The S-doped nanoparticles and nanofibers showed higher H₂S degradation activity as compared to pure nanoparticles and nanofibers where results showed that nanofibers have 10% higher efficiency than nanoparticles.

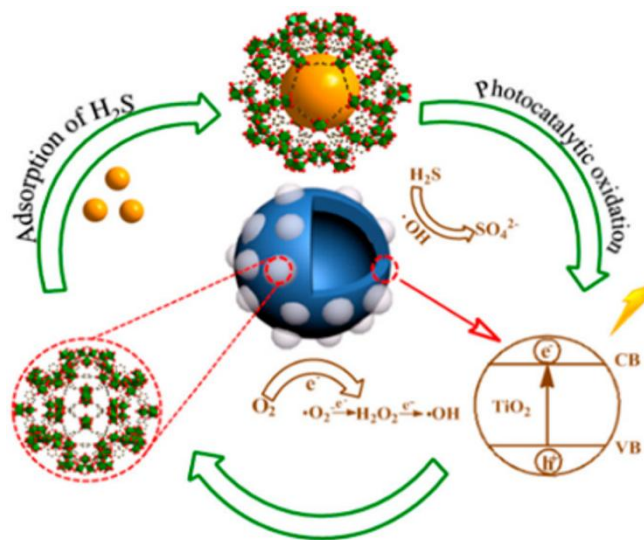
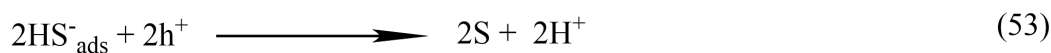
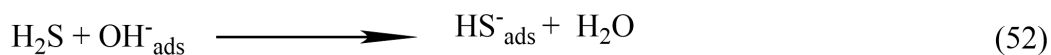
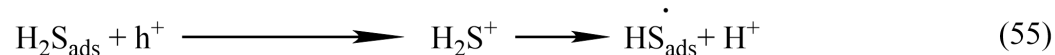


Figure 13. Schematic of the Reaction Mechanism for the removal of H₂S [202]. Copyright 2017 American Chemical Society.

Photocatalytic decomposition of hydrogen sulfide with the evolution of hydrogen gas was discussed by Bhirud et al. [204] as follow (Equations 52-58):



The process of photocatalytic oxidation is more favourable for energy revolution because it does not form the explosive hydrogen gas,



The resultant PCO product of H₂S is sulfate, which leads to SO_x conversion.



7. Modification techniques

Ultraviolet light only consists of 4-5% of solar spectra whereas visible region accounts for about 40% of the solar photons. For the preparation and development, visible light reactive photosensitizing dyes are adsorbed on the TiO₂ surface where the photosensitizing dye in this system is photochemically and thermally unstable [26, 205]. In the early 90's, Grätzel used a dye photosensitize TiO₂ electrode for the preparation of solar cell [206]. Since then, various studies have been conducted such as the reports of Borgarello et al [207], Hoffman and Bahnemann [208], who synthesized visible light-responsive photocatalysts by using different cations and metal oxides in a small quantity, but some limitations were also reported.

In advanced research, metal-ion implantation methods have been applied by using high-energy metal ions to change the electronic properties for the synthesis of doped-TiO₂. Apno et al. [209] studied implantation of TiO₂ by using numerous transition metal ions such as Fe, V, Cr, Co, and Ni at high voltage of 50-200 keV, which shifts the absorption band in the visible spectrum for these photocatalysts. In recent studies, the chemical doping method was used to improve the electronic properties of TiO₂ for the synthesis of visible light reactive TiO₂ by using metals, metal ions, non-metals and metal oxides [182].

7.1 Metals Doping

7.1.1 Transition and Noble Metals Doping

The TiO₂ doped by transition metals like V, Co, Cr, Fe and Ni, shifts the spectrum of TiO₂ to the visible band region and enhances the photocatalytic behavior of TiO₂ [210]. Transition metals can decrease quantum efficiency by providing the sites for charge recombination for photoinduced charge carriers. Transition metals doped anatase TiO₂ show thermal stability [211]. The doping of transition metals on TiO₂ can form a new level between the valence band and conduction band, which shifts the spectrum towards the visible region.

Photocatalytic behavior depends upon the nature and quantity of the doping agent. Kang [212] reported that metal doping not only decreases the band length and increases the photocatalytic activity of TiO₂, but it also cannot destroy the framework of TiO₂ the only drawback is that the metal remaining on the surface of TiO₂ can hinder the reaction sites. Morikawa et al.[213] studied the doping of Cr on TiO₂ for the degradation of NO. The result showed that the Cr doping could decrease the photocatalytic performance on the other hand doping of Cr with V on TiO₂ can improve the photocatalytic activity of the TiO₂ catalyst.

Doping of TiO₂ with transition metal ions can increase the photocatalytic response under visible light. Earlier, Choi et al. [214] investigate the 21 transition metal ions doped on TiO₂ to study the photocatalytic oxidation of chloroform and photocatalytic reduction of tetrachloride. It was reported that Fe³⁺, Mo⁵⁺, Ru³⁺, Os³⁺, Re⁵⁺, V⁴⁺, and Rn³⁺ ions increased the photocatalytic degradation of CHCl₃. Yan et al. [215] doped cerium metal ion on TiO₂ by sol-gel method. It was investigated that Ce doping forms an energy band between valence and conduction bands. This avoids the recombination of electron-hole pairs by capturing the photo-generated holes, while the electrons in this energy band can easily jump to the conduction band of TiO₂. As shown in Figure 14, Ce doping increases the photocatalytic activity of TiO₂.

Iron in a trivalent state was doped on TiO₂ by sol-gel hydrothermal method, the titanium metal (Ti⁴⁺) in TiO₂ is substituted by Fe⁺³ thus the concentration of Fe⁺³ decreases from the surface and shifts towards the TiO₂ deep bulk. It was also studied that doping concentrations and structures have significant influences on the doping of Fe on TiO₂. Cr and V also show good performance as a metal for TiO₂. The 3d electrons of Cr³⁺ jump to the conduction band of TiO₂, thus increasing the visible light absorption ability of Cr-TiO₂ for the photodegradation of active yellow XRG dye [216]. The V⁴⁺ can be doped on TiO₂ by different methods such as the sol-gel, flame spray pyrolysis (FSP) [217] and by other chemical methods [218]. TiO₂ doped with V⁴⁺ shift the conduction band of TiO₂ towards the visible light spectrum, thus V⁴⁺ ion increases the visible light-induced photocatalytic activity of TiO₂ [219].

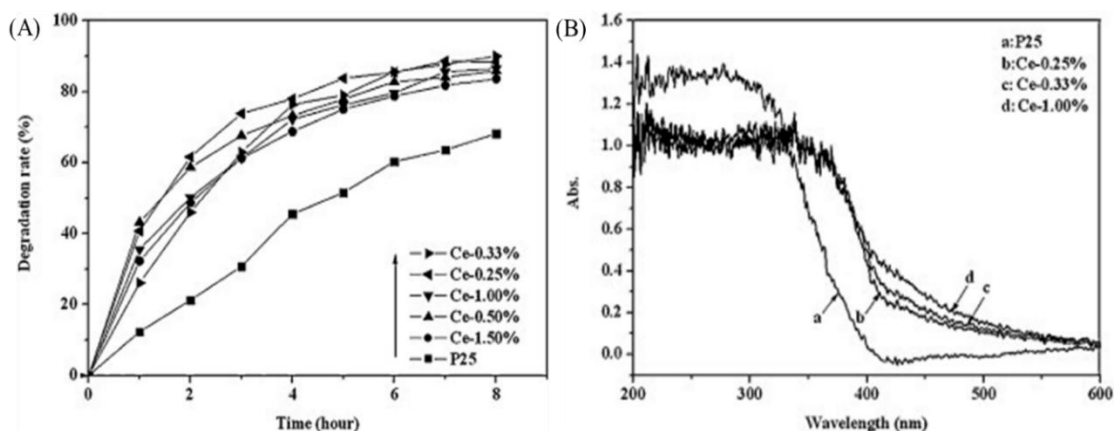


Figure 14: (A) UV-VIS spectra of Ce-TiO₂ samples with different Ce ion doping concentrations. (B) Curves showing the methylene blue degradation by Ce-TiO₂ catalyst with different Ce ion doping concentrations [215]. Copyright 2012 Elsevier.

Sn⁴⁺ doped TiO₂ replaces the Ti⁴⁺ ion in the TiO₂ lattice, causing the expansion of the lattice in *a* and *c* directions and changing the binding energy [220]. Zhuang et al. [117] investigated the Sn²⁺ doped anatase TiO₂ nanoparticles by using the sol-gel approach for the photodegradation of benzene under UV irradiations. The Sn²⁺ doped anatase TiO₂ nanoparticles

showed good photostability when examined for six days in a constant cyclic run. TiO_2 doped with Sn^{4+} enhances the hydroxyl group on the surface and the oxygen vacancies absorb in the UV light spectrum region. The results showed that the Sn^{4+} doping enhances the visible light absorption on TiO_2 [221]. The Ti^{3+} doped TiO_2 has also been studied and published.

Noble metals like Pd, Ag, Pt and Au can behave as electron trappers and increase the photocatalytic activity by transferring the charge and inhibiting the recombination of electron-hole pairs [213]. Hwang et al. [222] described that the Pt doped on the TiO_2 can enhance the transfer of the photo-generated electrons. Au-Pt alloy doped on the TiO_2 nanocomposite was studied by Fenglong Wang and coworkers [223] and its photocatalytic performance was compared with undoped TiO_2 . Results showed a tenfold increase in the photocatalytic activity of Au-Pt alloy doped TiO_2 . Choi et al. [224] studied the photocatalysis and dark reaction for the decomposition of organic pollutants such as 4-chlorophenol (4-CP) under UV irradiations using Ag/ TiO_2 and reduced hexavalent chromium (Cr (VI)) in the dark. The intermediates were formed by the photocatalytic oxidation of 4-CP where electrons stored in Ag/ TiO_2 were used for the reduction of Cr (VI). Karmaoui et al. [225] investigate the noble metals Ag, Pt and Au for the photocatalytic and plasmonic gas sensing to degrade NO_x . The Au-doped anatase- TiO_2 showed high photocatalytic activity for the degradation of NO_x as compared to other noble metals doped TiO_2 (Figure 15).

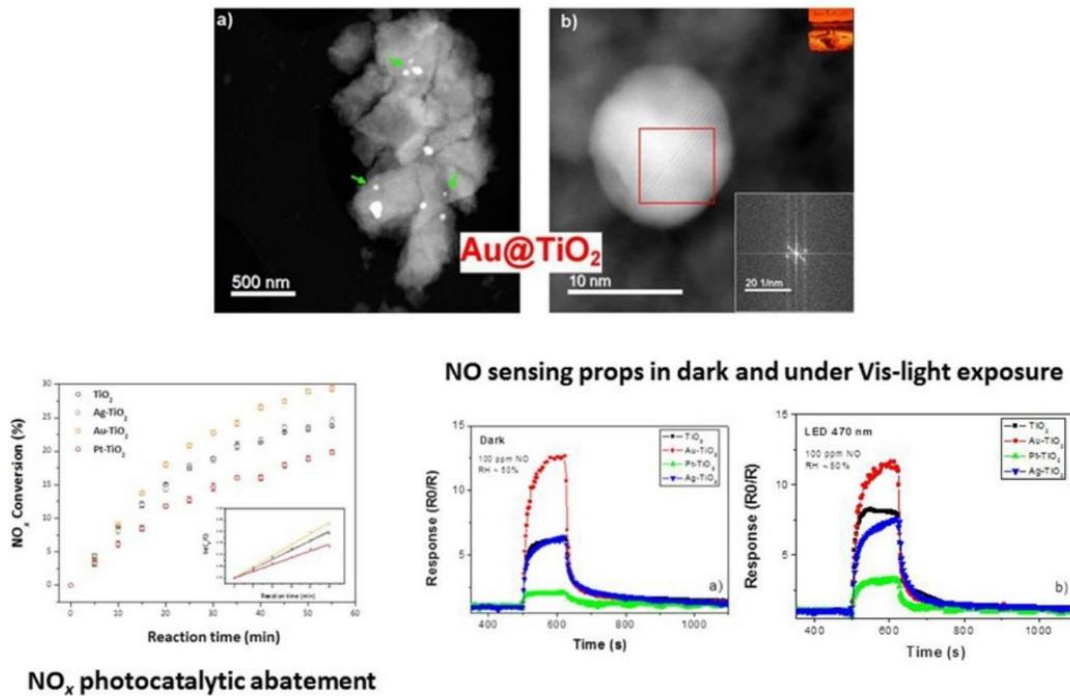


Figure 15: Noble metals modified TiO₂ NPs [225]. Copyright 2017 Elsevier.

7.1.2 Rare-Earth Metals Ions Doping

So far, there has been a lot of work reported on rare-earth metals like lanthanide doped on TiO₂ [226]. Sun et al. [227] studied La doping on TiO₂ and its substitutional effect on the electronic state of TiO₂ and its photocatalytic activity by using the density function theory (DFT) method. It was observed that the increase in visible light absorption and photocatalytic activity is attributed to the adsorption of La doping rather than replacing La doping. Zhang et al.[228, 229]studied the photocatalytic activity of Sm, Eu and Yb dopants on TiO₂. Sm-doped TiO₂ was synthesized by the chemical co-precipitation method. It was observed that the electrons from Ti⁴⁺ jump into the electronic structure of Sm³⁺, increasing the binding energy of Sm³⁺. The Yb-doped TiO₂ was prepared by the use of evaporation induced self-assembly process, and the

results showed that (1) Yb decreased the recombination of photoelectrons and holes, increasing the photocatalytic activity, and (2) the Yb dopant also stabilized the mesoporous structures.

Anandan et al. [230] reported the La-doped TiO₂ which under visible light irradiations reduces the recombination of electrons and holes and thus can photodegrade the salicylic acid. Parida and Sahu [231] doped La³⁺, Pr³⁺ and Nd³⁺ on TiO₂ and studied their photocatalytic activity towards Cr (VI) and methylene blue. La³⁺ doping on the mesoporous surface of TiO₂ enhanced the surface area, reduced the crystalline size and inhibited the TiO₂ phase transformation. Results showed that the photocatalytic degradation of Cr (VI) and methylene blue was increased by doping rare earth metals ions (La³⁺, Pr³⁺ and Nd³⁺) on TiO₂, while the highest photocatalytic activity was shown by La³⁺.

El-Bahy et al. [232] synthesized rare earth metal ions (La³⁺, Nd³⁺, Sm³⁺, Eu³⁺, Gd³⁺ and Yb³⁺) doped TiO₂ by sol gel technique. Lanthanide ions doped TiO₂ showed the highest photocatalytic activity for the photodegradation of organic dye as compared to pure TiO₂, where Gd³⁺ doped TiO₂ showed the promising photocatalytic activity among other lanthanide ions doped TiO₂ (Figure 16). Baiju et al. [233] reported the Gd³⁺ doped TiO₂ photocatalyst prepared by the sol-gel method showed higher photocatalytic activity than undoped TiO₂.

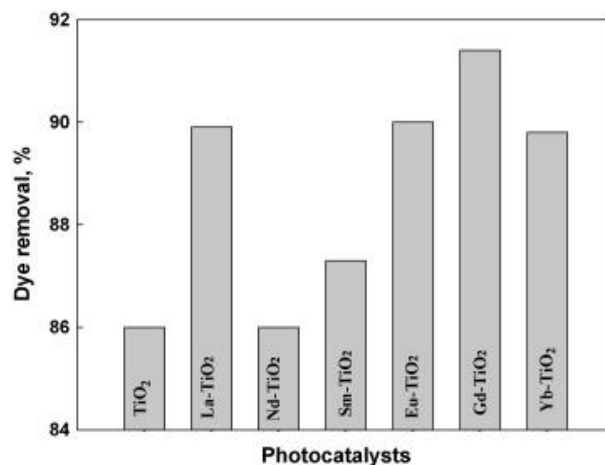


Figure 16: Effect of lanthanide ion-doped TiO₂ on the photodegradation of DB53[232].
Copyright 2009 Elsevier.

7.2 Non-Metals doping

Non-metals ions doping on TiO₂ is a hot topic for researchers nowadays. Due to the high cost and poor thermal stability of metal ions dopants, the use of non-metals has recently attracted wide attention from scientists to the band gap modification of TiO₂. Boron(B), carbon(C), nitrogen(N), sulfur(S), fluorine(F) and other non-metals having atomic radius equal to an oxygen atom [78]. Among all the non-metals N has attracted the interest of researchers and it has widely been studied due to stability and low ionization energy.

7.2.1 Nitrogen doping

Earlier N-doped compounds were prepared and studied under visible light to check the photocatalytic activity to their parent species [234, 235]. Later, Sato discovered the visible light-responsive material through the calcination of NH₄OH and TiO₂ solution [236]. Asahi et al. [78] reported that N doping TiO₂ increased the photocatalytic activity of TiO₂ by increasing the visible light absorption. After further investigations, it was studied that N-doped TiO₂ within the bulk enhanced the photocatalytic degradation of 2,4-dichlorophenol under visible light, while chemically absorbed N is harmful to the photocatalysts (Figure 17A) [237]. It was also reported that the source of N has beneficial effects on the doping of N. Urea, triethylamine, thiourea, and hydrazine hydrate are the sources used for N doping on TiO₂ by using the microemulsion-hydrothermal method [238]. Among these triethylamines are the most favorable source for N doping on TiO₂ showing the highest peak for photo-induced degradation of Rhodamine B under visible light as shown in (Figure 17B). N-TiO₂ can be prepared in two simple steps: firstly, to

synthesize TiO_2 and then doping with N by using an N-containing source at a high temperature [239] or using a nitrogen precursor inductivity-coupled plasma [240].

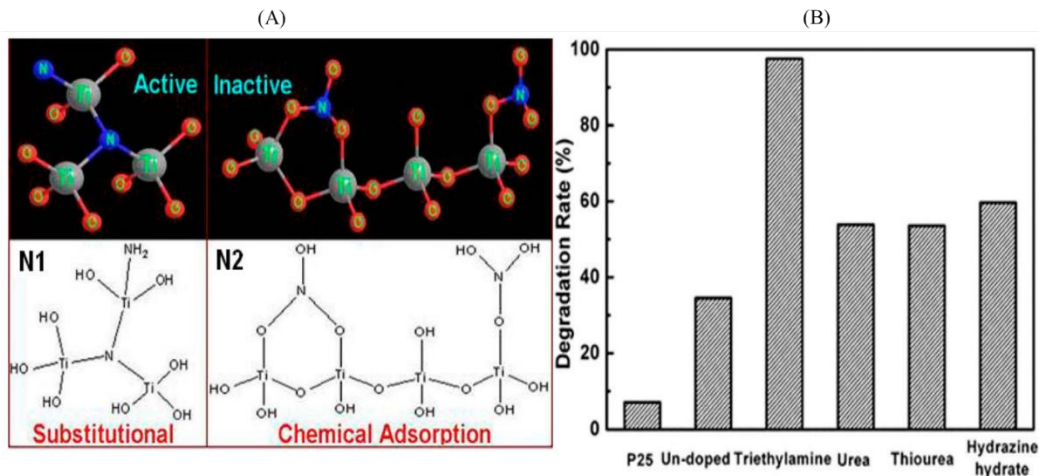


Figure 17: (A) Left part of the figure shows how nitrogen may be present in N-doped TiO_2 [190]. Copyright 2009 Elsevier. (B) The right part of the figure shows the photocatalytic activities of N-doped TiO_2 prepared from different nitrogen sources at the respective optimal doping values [238]. Copyright 2007 American Chemical Society.

For significant N doping on TiO_2 on the surface or bulk, both dry and wet methods have been used. Nitrogen ions can directly react with TiO_2 using physical techniques such as ion implantation [241, 242] and sputtering [243, 244], other techniques like atomic layer deposition [245], gas phase reactions [246, 247] and pulse-layered deposition [248] have also been used for the synthesis of N-doped TiO_2 . The most promising method for the preparation of N-doped TiO_2 nanoparticles is the sol-gel technique which requires an easily operating machine which controls the porosity and morphology of the nanoparticles. Titanium salts (TiCl_4) and alkoxide precursors (titanium tetra isopropoxide $\text{Ti}[\text{OCH}(\text{CH}_3)_2]_4$, tetrabutylorthotitanate $\text{C}_{16}\text{H}_{36}\text{O}_4\text{Ti}$) are used for the growth of N doping. In addition to the aforementioned titanium alkoxide is also

hydrolyzed for N doping with the source of nitrogen, e.g., aliphatic amines, ammonia, ammonium salts, nitrates and urea [249, 250].

To enhance the nitrogen quantity in the lattice of TiO_2 , Ti^{4+} is treated with ligands having N like Ti^{4+} -amine complexes or Ti^{4+} -bipyridine [251]. Another way for N doping is to react with urea, and the N is doped during the condensation process of the alkoxide precursor, shifting the spectrum towards the visible region (3.2 to 2.3 eV). Sol-gel technique is used to synthesize the visible light active TiO_2 nanostructure doped with N surfactant. Simply, visible light active N- TiO_2 is formed by using dodecylammonium chloride (DDAC) (Figure 18) [252]. The pore-templating material DDC simultaneously changes the structural properties. Hence the N-doping activates the TiO_2 for visible light absorption and increases its photocatalytic activity, reactivity and functionality for various environmental applications [253, 254]. The most reported and published research on N-doped TiO_2 may occur on the polymeric anatase form of N-doped TiO_2 . The anatase-rutile mixed form was also synthesized and was made visible light active by changing the parameters of the sol-gel method [237]. Such a combination of anatase-rutile photocatalysts transfers the electrons from anatase to rutile by photoexcitation, decreasing the recombination of electrons and holes and increasing the photocatalytic activity under visible light irradiations. synthesized N doped.

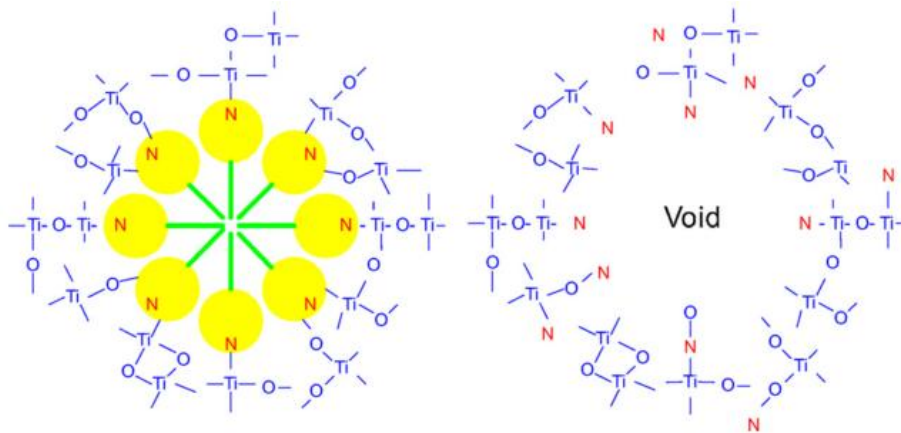


Figure 18. Templating sol-gel method utilizing nitrogen-containing surfactants as both nitrogen source and pore template material [252]. Copyright 2007 American Chemical Society.

Anatase/rutile TiO_2 photocatalyst which showed nine times greater photocatalytic activity with a high range of λ greater than 430nm as compared to Evonik P25. Plasmonic Au/TiO_2 was synthesized for the photodegradation of formaldehyde by single pass continuous flow reactor under visible light. The highest activity of 83.3% formaldehyde conversion was noted when the air was wet and the rate of humidity (RH) was equal to 44%, while in dry air, Au/TiO_2 became inactive even under the visible light irradiations (Figure 19) [256]. The situ DRIFT studies revealed that the formaldehyde oxidization terminated at Dioxymethy I (DOM) production in a dry environment and the presence of TiO_2 . For Au/TiO_2 , formaldehyde oxidation stops at format and carbonate without the formation of CO_2 in the dark, while in the wet air, the continuous formation of CO_2 was noted. Linsebigler et al. [221] studied that treating TiO_2 with NH_3 for N doping under visible irradiations by calcination method increased the photocatalytic activity while doping TiO_2 with N_2 reduced the photocatalytic activity due to the widening of the bandgap. Hirai et al. [257] synthesized mesoporous N doped TiO_2 by calcination method which showed better performance due to large surface area than doped TiO_2 prepared by sol-gel technique under visible irradiations.

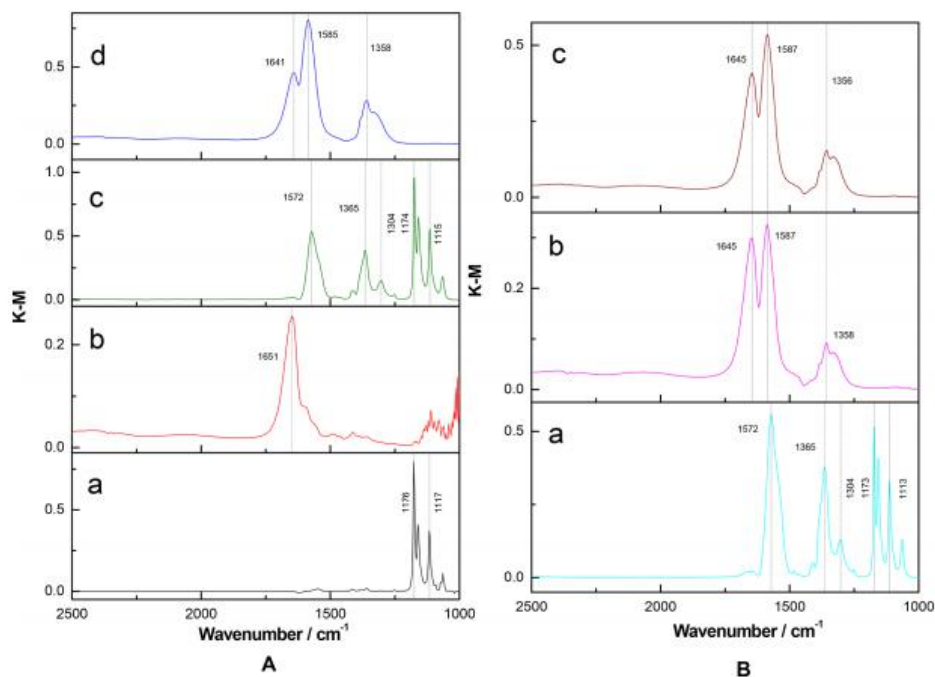


Figure 19. In situ DRIFT spectra at wavenumbers between 2500 and 1000 cm⁻¹ of formaldehyde oxidation (A) at 120 min of TOS under dark at (a) dry, (b) wet over TiO₂, and (c) dry, (d) wet over Au/TiO₂; (B) at 90, 180, and 210 min of TOS under subsequent conditions of (a) light and dry, (b) light and wet, and (c) dark and wet over Au/TiO₂, respectively [256]. Copyright 2017 American Chemical Society.

7.2.2 Carbon Doping

Carbon has also been reported as an active dopant for visible light utilization and photocatalytic performance of TiO₂. Nagaveni et al. [258] prepared C-doped TiO₂ using sol-gel techniques for the photocatalytic degradation of methylene blue under UV-Vis irradiation. Kamisaka et al. [259] studied the structural and optical properties using the DFT technique. The DFT results showed that by C doping four structures were assumed to be obtained. Among them, Ti and O, the substitutes of C doping, have not found any clues for visible light utilization due to titanate anions formation. On the other hand, C doping substitutes O⁻ and does not cause

any change in the structure, which is beneficial for TiO_2 to absorb visible light. Xia et al [260] synthesized a monodispersed C doped rutile TiO_2 hierarchical structure uncovered facet (110) for the evolution of H_2 photo catalytically from water. About 450 mL of H_2 was released in 196 min. Yu et al [94] prepared a novel type of C-doped TiO_2 with uncovered facet (001) sheets by a hydrothermal method having enhanced efficiency for the absorption of the entire visible range along with redshift edge. Lin et al [261] prepared novel visible light-responsive C-doped mesoporous TiO_2 by using sol-gel and hydrothermal methods for the photodegradation of the dye-reactive bright Red X-3B.

7.2.3 Fluorine Doping

Doping of F on TiO_2 is the most interesting topic which has recently attracted the attention of researchers, where the direct doping of F on TiO_2 for photocatalytic degradation activity using a UV-VIS source is rather controversial [262, 263]. In the solvothermal process, fluoride ions are doped on the TiO_2 photocatalyst surface, rather than in the lattice. A single-step solvothermal method was adopted using a hydrophobic NH_4F modifier and an isopropanol solvent to form super hydrophobic mesoporous MCF doped with fluorinated TiO_2 nanoparticles [264]. The synthesized photocatalyst exhibits an enhanced photocatalytic activity, high adsorption, and super hydrophobic properties for the degradation of Rhodamine B degradations as shown in Figure 20. It was reported that the substitution of F in the TiO_2 lattice neither introduces impurity nor shifts the band gap [265]. However, when studying SnO_2 and ZnO_2 , it turns out that the replacement of oxygen vacancies by F would introduce impurities in the band gap [266]. It was summarized that F was substituted in the O vacancies which remove the recombination sites to induce vacancies and impurities in the TiO_2 lattice [267].

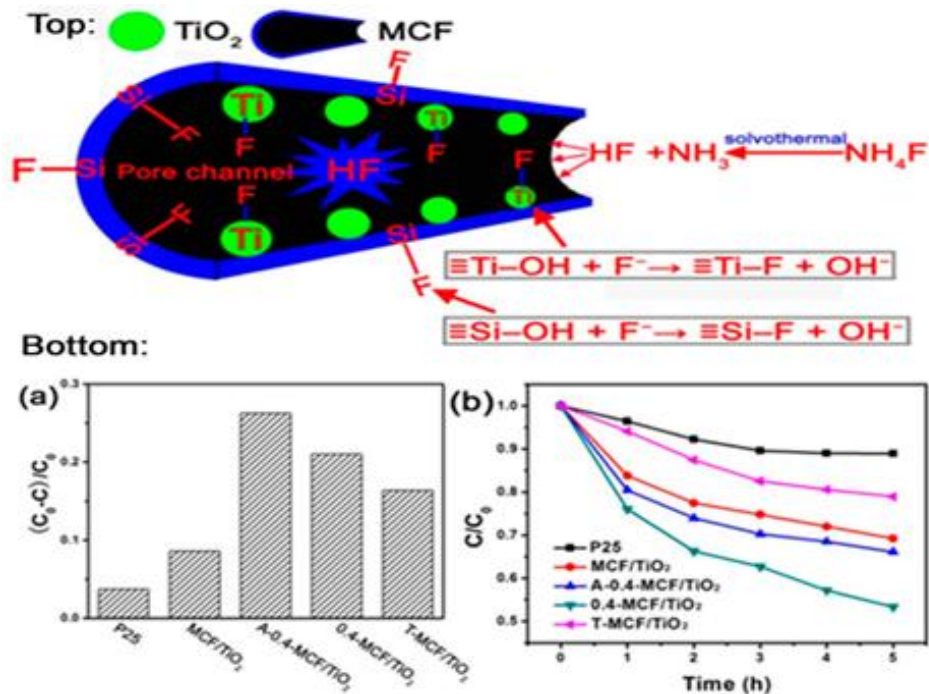


Figure 20. The top figure shows a schematic diagram of the fluorination reaction occurring in the pore channels of MCF; the bottom figure shows the adsorption capacities of RhB (20 mg/L, catalyst concentration: 0.25 g/L) on different samples (a); visible light photocatalytic activities of different samples (b) [264]. Copyright 2012 Elsevier.

7.2.4 Sulphur Doping

Due to the larger ionic radii sulfur addition in the TiO₂ lattice, is difficult as compared to N. Cationic sulfur (S⁶⁺) may be chemically easily inserted than anionic sulfur (S²⁻). Periyat et al.[268] synthesized cationic-anionic doped TiO₂ using ammonium sulfate by sol-gel method. In other work of the same group [269], it was also reported S doped TiO₂ by modifying titanium isopropoxide (Ti[OCH(CH₃)₂]₄) using H₂SO₄. It was concluded that the anatase was maintained at a high temperature (≥800°C) through the formation of titanyl oxysulfate (TiOSO₄). Thus, the presence of sulfur increases the photocatalytic activity of the synthesized materials under visible light irradiations. Han et al.[270] prepared the visible light active S-doped TiO₂ film from

non-ionic surfactant and H_2SO_4 as an inorganic source of sulfur using a novel sol-gel technique based on a self-assembled method. Both anionic S^{2-} and cationic species S^{6+}/S^{4+} were doped uniformly on the surface of the S-doped TiO_2 film. Due to the doping of anions or oxygen vacancies, strong EPR significantly limits the energy band in TiO_2 . For the photocatalytic degradation of microcystin-LR (MC-LR), the most reliable photocatalyst is mesoporous S-doped TiO_2 under visible light irradiations (Figure 21).

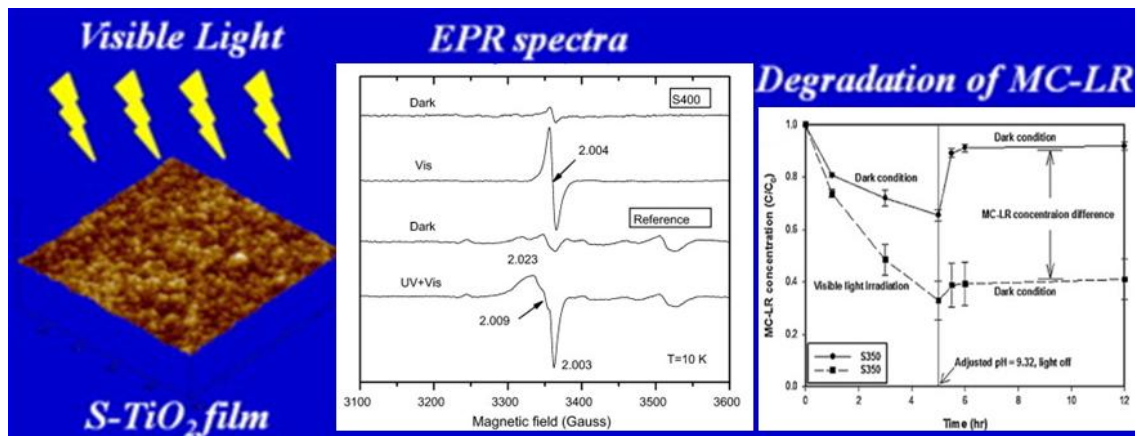
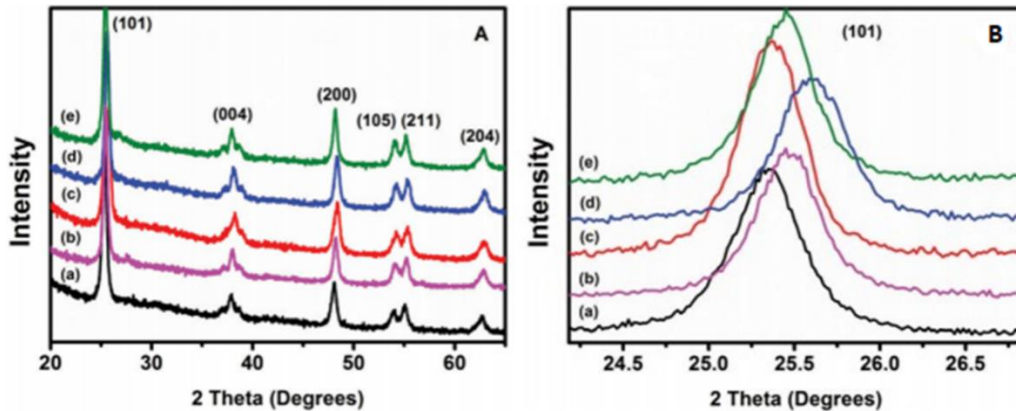


Figure 21: Visible light-activated sulfur-doped TiO_2 films for water treatment[270]. Copyright 2011 Elsevier.

7.2.5 Boron Doping

Compared with other non-metals, TiO_2 is rarely doped with boron. While investigating B-doped TiO_2 , it was observed that the absorption of visible light leads to redshift, which causes the overlapping of 2p electrons of O with the impurities of B. Besides this, it was also studied that the B-doped TiO_2 showed a spectrum in the blue shift instead of the red shift that reduced the size of the crystal (Quantum size effect) due to the presence of B [271, 272]. Miguel et al.[273] prepared an interstitial boron-doped TiO_2 thin films and found an improvement in the

photocatalytic activity of TiO_2 . The promising effect of coating B on TiO_2 increases the atmospheric chemical vapor pressure deposition which thus enhances the photocatalytic activity of $\text{B}_{\text{int}}\text{-TiO}_2$. Stengl et al. [274] synthesized B-doped nanosized TiO_2 by the reaction of TiOSO_4 with urea and amorphous boron by the process of homogenous hydrolysis followed by annealing at 700°C . Results showed that B-doped TiO_2 owing to the better utilization of visible light have good photocatalytic activity as compared to reference TiO_2 . Recently, researchers have been interested in studying the modification of TiO_2 by boron and other co-dopants and non-metallic ions [275, 276]. Nasr et al. [277] synthesized highly active BN/TiO_2 nanofibers for the degradation of methyl orange by the electron spinning method. The results indicated that the BN coating on TiO_2 nanofibers increased the band gap between electrons and holes as compared to pure TiO_2 nanofibers. Compared with TiO-P25 and TiO_2 nanofibers, the photodegradation of methyl orange under UV irradiation of BN/TiO_2 is increased by 5 times and 3.8 times, respectively (Figure 22).



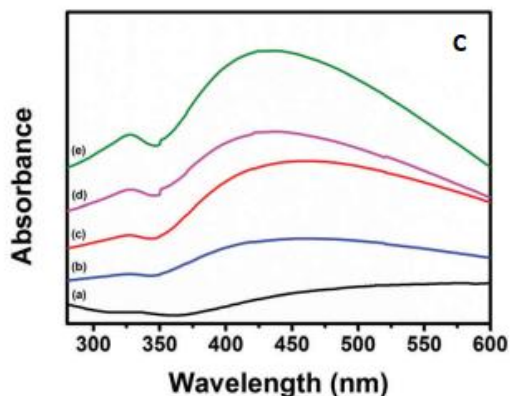


Figure 22: (A,B) XRD pattern (C) UV-VIS absorption spectra of (a) TiO₂, (b) BN (3 wt%)/TiO₂, (c) BN (5 wt%)/ TiO₂, (d) BN (7 wt%)/TiO₂ and (e) BN (10 wt%)/TiO₂ annealed nanofibers in air for 4 h at 500 °C [277]. Copyright 2018 Royal Society of Chemistry.

7.3 Co-doping

To improve the photocatalytic performance of TiO₂, multiple components were used, i.e., co-doped to modify TiO₂ to utilize the visible spectrum region of sunlight. Co-doping of TiO₂ is the recent interest of researchers in the field of photocatalysis. It was reported that the co-doped TiO₂ has a higher photocatalytic activity as compared to singly doped TiO₂ due to the synergistic effect and electron/hole separation [227, 229, 278-280]. According to the band theory for semiconductors, it was explained that the Ti contributes its 3d energy orbital while the oxygen shares its 2p orbital to form a valance band of TiO₂ while the other doping non-metals impurities like N, C, S, P and F also contributes there 2p orbitals having much higher negative energy substitute in the lattice of oxygen along with other non-metal dopants. Thus, new energy bands are formed above the TiO₂ valance band which facilitates the utilization of visible light and increases the photocatalytic activity of TiO₂ [26]. Cong et al. [281] suggested the energy levels of 1s energy orbital of C doping and 1s energy orbital of N doping in the valance band for co-doping of TiO₂. The band gap of TiO₂ became smaller while the visible light photocatalytic activity enhanced. Liu et al. [282] and In et al. [283] investigated the B and N co-

doped TiO₂ (Ti-B-N) on the surface have higher photocatalytic activity and showed higher absorption of UV-Vis light. Bikramjeet Singh and coworkers [284] studied BN-doped TiO₂ for the photodegradation of methylene blue. The large surface pores favor the catalytic oxidation reactions. Decrease of the band size, higher photocatalytic activity, pore structure optimization and reusability were due to B-O-Ti-O. Results showed that BN-TiO₂ photodegrade the 79% methylene blue in 200 min, while pure TiO₂ degrades 32% under visible light (Figure 23).

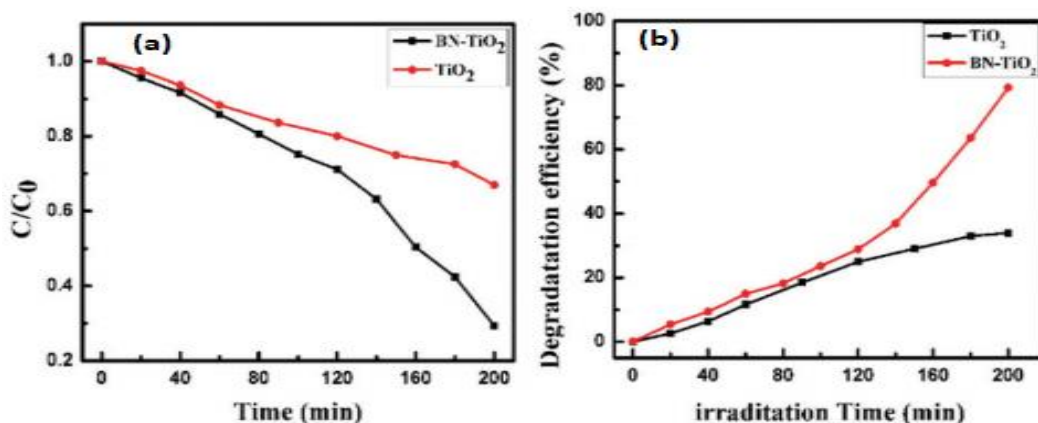


Figure 23: (A) Concentration vs. irradiation time and (B) degradation efficiency vs. irradiation [284]. Copyright 2017 Royal Society of Chemistry.

Komai et al. [285] reported the N and S co-doped TiO₂ having improved photocatalytic activity for the degradation of methylene blue under visible irradiations. It was proposed that the N and S could form an anodic co-doping thereby narrowing the band gap of TiO₂ and thus enhancing its photocatalytic activity by increasing the visible light absorption. Yang et al. [286] proposed the S and F co-doped mesoporous TiO₂. By maintaining and controlling the structure and morphology, the ability of mesoporous TiO₂ to absorb visible light is enhanced with the decrease of electron-hole recombination. S and F co-doping absorbed visible light with the redshift and shows the ability to degrade many organic pollutants and dyes. N and F co-doped

TiO_2 microspheres have a synergetic effect on TiO_2 and were prepared by solvothermal technique [287]. It was proposed that co-doping of N and F on TiO_2 increased the photocatalytic activity and visible light-induced photodegradation of AO7. C and B co-doped TiO_2 prepared by gel hydrothermal method have also high photocatalytic activity due to the narrowing of the band gap because of B doping [288]. Vanadium, V and N co-doped TiO_2 showed higher photocatalytic activity under visible irradiations than singly doped TiO_2 and were synthesized by sol-gel technique. The increase in photocatalytic behavior is due to the shortening of the band gap by inducing V and B in the TiO_2 lattice [220]. Lanthanum, L and N co-doped TiO_2 not only have a higher photocatalytic activity under visible light but also reduce the recombination of electrons/holes and increase the surface area for better absorption of visible light irradiation, thereby improving its photocatalytic ability [289]. Biswas and co-workers [290] investigated the N and F co-doped TiO_2 nanoparticles and adjusted the ammonium fluoride-urea concentration and the reaction time at 300 °C between 1-7%. The results showed that N/F doped TiO_2 nanoparticles exhibited a higher redshift band spectrum of >600nm, where their colloidal dispersion was absorbed in UV to near IR irradiations. Reactive oxygen was produced in the presence of UV irradiation which was used for the photodegradation of toxic chemicals, pathogens, and cells (Figure 24).

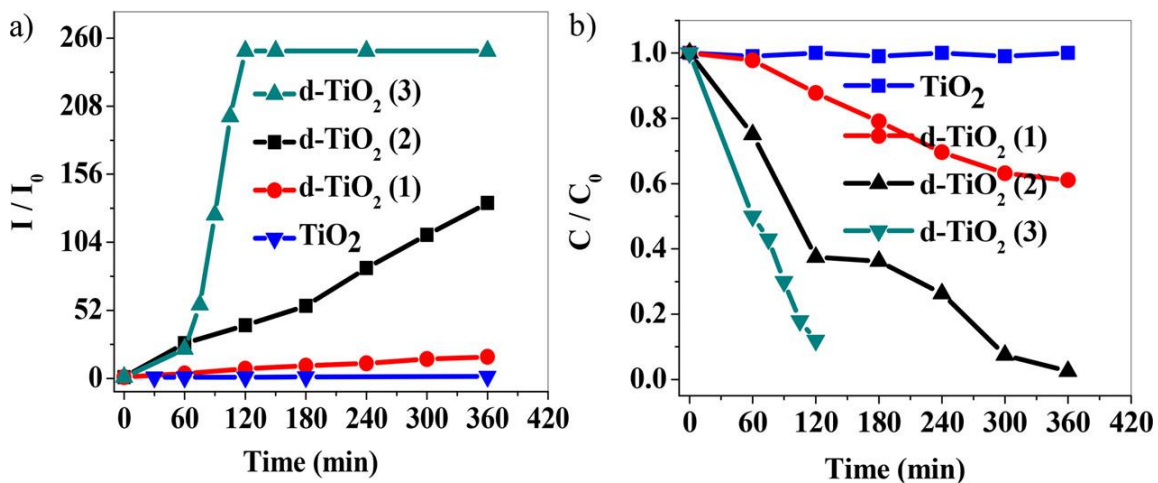


Figure 24: (A) Visible light-induced reactive oxygen species generation by N, F co-doped TiO₂ nanoparticle. (B) Visible light photodegradation of bisphenol A using N, F co-doped TiO₂ nanoparticle as photocatalyst showing that bisphenol A degradation kinetics by nanoparticles is in the order of d-TiO₂(3) > d-TiO₂(2) > d-TiO₂(1) > undoped TiO₂ [290]. Copyright 2017 American Chemical Society.

Cong et al. [291] synthesized N and 0.5% Fe³⁺ co-doped TiO₂ for the first time using homogeneous precipitation hydrothermal technique, thereby lowering the band gap of TiO₂ and increasing the separation between electrons and holes. Such N and Fe³⁺ co-doped TiO₂ showed better photocatalytic activity as compared to pure TiO₂ with an increase of 5% under UV light and 75% under visible light irradiations. Wong et al. [292] reported that doping of Ag on the surface of N-doped TiO₂ improved the visible light absorption ability. Wang and coworkers reduced the limitations by sandwiching Ag between [TiO₂(N)] like TiO₂(N)/Ag/TiO₂(N). Hoang et al. [293] reported the higher photocatalytic activity of co-doped Ti³⁺ and N on TiO₂ nanowires. The oxidation state of N is lower but occupies a higher energy level due to the Coulombic force. Thus, electrons of singly N-doped TiO₂ can be excited with high energy longer wavelength photons. Dhandole et al. [294] studied the Rh and Sb co-doped visible light active nanorods of rutile (Rh–Sb: TiO₂ NR) for the photocatalytic degradation of organic pollutants and microbial pathogens. To improve and increase the photocatalytic activity of Rh–Sb:TiO₂ NR was treated with acid and Cu_xO (Cu_xO/A–Rh–Sb:TiO₂ NR). The results showed that the Cu_xO/A–Rh–Sb:TiO₂ NR photocatalyst was eco-friendly and had a high capability for the removal of environmental organic pollutants and microbial pathogens inactivation (Figure 25).

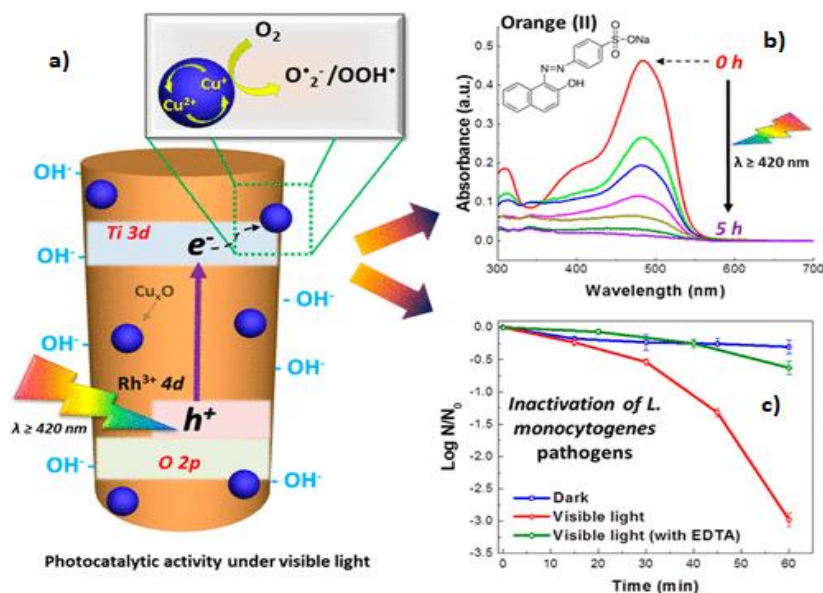


Figure 25: (A) Schematic diagram of photocatalytic degradation of Orange (II) dye by copper oxide loaded A-Rh-SbTiO₂ NRs under visible light irradiation, (B) Orange (II) dye degradation under visible light absorbance spectrum of 2 wt % of Cu_xO/A-Rh-Sb:TiO₂ NR, (C) Inactivation of *L. monocytogenes* using Cu_xO/A-RhSb:TiO₂ NRs in dark condition, visible light condition and visible light with EDTA [294]. Copyright 2018 American Chemical Society.

7.4 Modification of Oxygen-Rich TiO₂

Recently, oxygen has been generated by per oxo titania complex using situ thermal decomposition [295]. This process enhanced the strength of the Ti-O-Ti bond, thereby mounting the valance band (VB) shifts and thus increasing the visible light absorption ability. The upward shift of VB due to oxygen-enriched TiO₂ is the main factor for the increased visible light absorption capability which in turn increases the photocatalytic activity. Oxygen-rich TiO₂ and controlled TiO₂ were synthesized as shown in Figure 26.

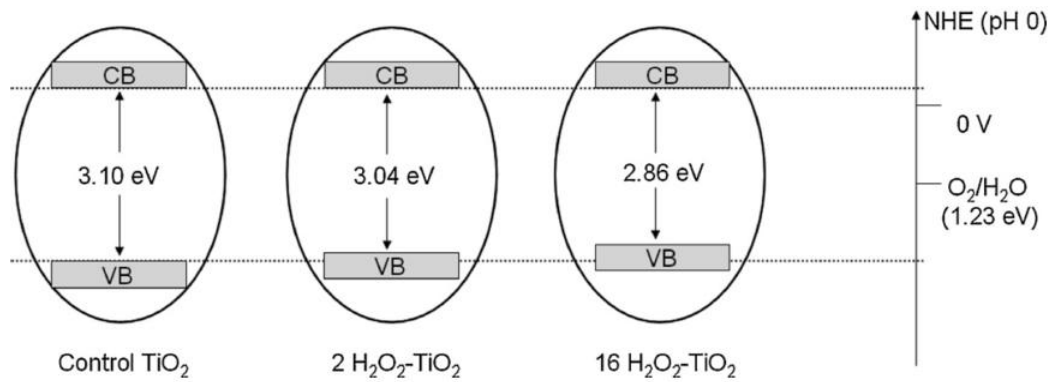


Figure 26: Mechanism of band gap narrowing by oxygen excess [295]. Copyright 2011 Wiley.

8. Kinetic studies on the photodegradation of gaseous pollutants

The rate of the photocatalytic reaction depends on the pollutant molecules covering the surface of the catalyst particles at a steady state. That's why, the adsorption modelling and the kinetic modelling look nearby similar, thus literature studies showed the wide applications of the Langmuir-Hinshelwood (LH) relationship for this purpose. LH is used in the photocatalytic reactors for the local light effect,

$$-r_p = \frac{[I(x,y,z)]^n k K C_{p,s}}{1 + K C_{p,s}} \quad (52)$$

Where the apparent rate constant is denoted by k , Langmuir adsorption equilibrium constant by K , the impurities concentration at the catalyst surface is denoted by $C_{p,s}$. The concentration of pollutants in the bulk fluid is equal to the concentration of the pollutants adsorbed on the surface in the absence of mass transfer limitation. Researchers explored that no mass would transfer unless the rate of the reaction is independent of the air volume flow rate in the reactor. Nevertheless, the simple model to transfer the mass and rate of photocatalytic reaction and has a constant area of cross-section [296]. The n in the equation above is the intensity of the

incident light. The higher the incident light, the greater the recombination of electrons and holes ($n < 1$), whereas the lower the intensity of light, the stronger the degradation of pollutants ($n=1$). When the concentration of the pollutants is small the above equation (52) becomes [297],

$$-r_p = [I(x,y,z)]^n k' C_p, s \quad (53)$$

Three different types of equations i.e., namely the two types of sites where the LH bimolecular competes and the two types of sites where the LH bimolecular does not compete and were obtained by the expansion of LH model due to the water vapor adsorption competition (Equations 54-56)[296, 298-300].

$$-r_p = [I(x,y,z)]^n k \left(\frac{K_p K_w C_p C_w}{(1 + K_p K_w C_p C_w)^2} \right) \quad (54)$$

$$-r_p = [I(x,y,z)]^n k \left(\frac{K_p C_p}{(1 + K_p C_p)} \right) \left(\frac{K_w C_w}{(1 + K_w C_w)} \right) \quad (55)$$

$$-r_p = [I(x,y,z)]^n k \left(\frac{K_p C_p}{1 + K_p C_p + K_w C_w} \right) \left(\frac{K'_w C_w}{(1 + K'_p C_p + K'_w C_w)} \right) \quad (56)$$

Where p in the subscript represents the water and pollutant. Thus, the above equations for certain reactors fit satisfactorily in the experiments but were not suitable for the reactions occurring on the surface of the catalyst. That's why if some authors used different reactors and operating systems, they can't compare their experimental data with the LH model. However, limitations were found when formaldehyde degradation was done on a monolith-type reactor [301, 302], used on glass plate reactor [303]. The Intrinsic parameters contained in the reaction

kinetic equations are independent of fluid dynamics, radiation field and reactor geometry. The reaction kinetic scheme was simplified by the addition of different species in a reaction.

Passalia et al. [304] studied formaldehyde degradation by using a single-pass plate photocatalytic reactor. The intrinsic kinetic model plausible reaction approach was applied to kinetic steady pathways that utilize the kinetic steady state approximation for the next generation of electrons and holes. The reaction rate model is used to replicate the experimental results obtained by the corrugated plate photocatalytic reactor [305-307]. Imoberdorf et al. [308, 309] investigated the degradation of perchloroethylene (PCE) by attacking the chlorine radical using the laboratory flat-scale plate for the derivation of intrinsic kinetic expression. Studying the TCE of the LH models in the literature showed effects on photocatalytic rate due to the concentration of water vapors and another equation for the degradation of TCE by the reaction of electrons and hole pairs in the absence of water vapors, exhibited the first-order reaction kinetics, linear TCE adsorption/desorption equilibrium, and steady-state concentrations of holes and adsorbed intermediates [310]. Proposed intrinsic reaction expression schemes for the degradation of toluene [311] and cyclohexane [312] have also been used. Hence, in the future, it is very important to use the intrinsic kinetic expression for the reaction mechanisms of scientific and engineering research.

9. Techniques for Immobilization of TiO_2

Immobilization of TiO_2 is a technique used to fabricate the reactors for air purification. Doping TiO_2 with supportive materials or TiO_2 fabrication into thin film. TiO_2 fabrication itself is an excellent technique for the immobilization of photocatalysts for air purification. Thevenet et al. [102] studied the PCO reaction for the elimination of acetylene by loading P25 TiO_2 on glass fibers. A 50% dry mixture of both P25 TiO_2 and colloidal silica was used for the synthesis and was loaded on silica glass fibers. Other supporting materials that can be used for immobilization of photocatalyst powders include graphene oxide [104], optical fibers [19], PVC sheets [105] or

monolith [103]. Antonello and coworkers [108] proposed gas phase PCO of VOCs by using the novel method for electrochemical fabrication of transparent and mechanically robust TiO₂ film. TiO₂ film showed self-cleaning and promising properties for the degradation of VOCs. Xie et al. [107] investigated the window glass PVP(polyvinylpyrrolidone) modified thin film TiO₂ by sol-gel method for the degradation of benzene and acetone. It was observed that the rate of decomposition increased due to enhanced crystallinity as compared to those reactions where PVP was not added.

The most important methods for immobilization of catalysts are chemical vapor deposition (CVD), sol-gel, thermal, layer-by-layer (LBL) and electrophoretic deposition methods (EPD). Support was introduced into the gaseous catalytic atmosphere by the chemical vapor deposition method at a high temperature which decomposed on the surface of support [313]. The N-doped TiO₂ was prepared by CVD method by using different precursors [247]. It has also been used to control the thickness of TiO₂ film [314] and TiO₂in situ crystallization [315, 316]. Glass plates and glass rings are used as catalyst support materials which fabricate with TiO₂ precursor and high calcination temperature (>450°C) in the sol-gel method. Sol-gel technique is cost-effective, flexible and available in a variety of shapes [313, 317, 318]. Recently, a hybrid sol-gel suspension method at low temperature (<150 °C) was introduced and applied on different substrates such as glass fibers, aluminium, Al₂O₃ monoliths, stainless steel, etc. to synthesize thick, highly photo-catalytically active and stable layers from various commercial TiO₂ nanoparticles [319].

In the thermal synthesis method, the catalyst is directly scattered onto the support and thermally treated [313, 320]. Catalyst performance depends upon the temperature of calcination which affects the physical properties of TiO₂ such as structure, crystal phase, oxygen adsorption capacity and BET surface area [321].The support material is dipped or sprayed several times in the colloidal solution of the catalyst till the desired layer is achieved. Catalyst and support are bound together electrostatically. The Nanoparticle's dispersion in the porous

matrix and thickness of the catalyst are controlled in the LBL method easily, thus, providing a high surface area without the need for high calcination temperature [322-325]. In the electrophoretic deposition (EPD) technique, charged particles move when an electric field is applied through stable suspension. In the EPD method, the thickness of the film is controlled, and it can also be used on complex shapes and is environmentally friendly. EPD can be used inside the array of TiO₂ nanotubes [326], for the deposition of chitosan/h-BN/ TiO₂ composite on metals [327], on a plastic substrate [328] and can also be used to coat the biological molecules in future [329].

10. Concluding Remarks and Perspectives

Pure TiO₂ can only be activated by using high-energy photons in the UV region having $\lambda \leq 387$ nm for anatase. This is due to the large band gap of pure TiO₂ although its practical use and applications are minimized [330, 331]. Different strategies were adopted to improve the photocatalytic performance of TiO₂. They include the modification in the morphology of TiO₂ such as enhancing the surface area and porosity, or chemical modifying the structure of TiO₂ by adding the components additionally. However, the performance of visible light active (VLA) TiO₂ can be improved by controlling the morphology of the semiconductor through the chemical modification method. The one-dimensional TiO₂ morphology is preferred due to its high surface area and reduction in the recombination process. Despite the progress and great interest of the scientists in the field of photocatalysis, still it cannot be commercialized due to some complications such as visible light absorption ability, low quantum efficiency, selectivity towards CO₂ and H₂O formation and stability. Combine work is needed in photocatalysis from different fields of specialization such as chemists, material scientists, chemical engineers and bandgap engineers [34].

Environmental pollution, especially VOCs and indoor air quality is a hot topic of attention for the scientist these days. The best way for the degradation of VOCs and refining

the quality of indoor air is PCO. Extensive research has been done to understand the charge separation and mechanism for the photodegradation of VOCs and other pollutants. TiO_2 is the most promising photocatalyst under UV irradiation. There is a great demand to develop a photoactive TiO_2 with doping or other methods to prepare the novel TiO_2 that can enhance its efficiency for the degradation of VOCs under visible light. Nano-scaled TiO_2 exhibited higher photocatalytic performance in PCO reactions and further efforts are required to modify them either by fabricating and analyzing them under different reaction conditions to achieve better performance and commercialization. Discovering different ways of doping and fabrication to modify nano-scaled TiO_2 is the current and future interest in research and further applications.

REFERENCES

1. Chen, D., et al., *Photocatalytic degradation of organic pollutants using TiO_2 -based photocatalysts: A review*. Journal of Cleaner Production, 2020. **268**: p. 121725.
2. Shayegan, Z., C.-S. Lee, and F. Haghghat, *TiO_2 photocatalyst for removal of volatile organic compounds in gas phase—A review*. Chemical Engineering Journal, 2018. **334**: p. 2408-2439.
3. Stucchi, M., et al., *Surface decoration of commercial micro-sized TiO_2 by means of high energy ultrasound: A way to enhance its photocatalytic activity under visible light*. Applied Catalysis B: Environmental, 2015. **178**: p. 124-132.
4. Alzaky, M.A.M., et al., *Yellow Phosphorus and Potash for SOX and NOX removal*. Environmental Technology, 2021(just-accepted): p. 1-26.
5. Kashif, M., et al., *Gallium oxide impregnated on porous clay heterostructures material for selective catalytic reduction of nitrogen oxide with C_3H_6* . Journal of Environmental Chemical Engineering, 2020. **8**(4): p. 103943.
6. Stefanov, B.I., et al., *Acetaldehyde adsorption and condensation on anatase TiO_2 : Influence of acetaldehyde dimerization*. Journal of Molecular Catalysis A: Chemical, 2014. **381**: p. 77-88.
7. Kim, S., et al., *Practical scale evaluation of a photocatalytic air purifier equipped with a Titania-zeolite composite bead filter for VOC removal and viral inactivation*. Environmental Research, 2021: p. 112036.
8. Pham, T.-D. and B.-K. Lee, *Novel adsorption and photocatalytic oxidation for removal of gaseous toluene by V-doped TiO_2/PU under visible light*. Journal of hazardous materials, 2015. **300**: p. 493-503.

9. Ohashi, S., et al., *Recent advances from basic and clinical studies of esophageal squamous cell carcinoma*. Gastroenterology, 2015. **149**(7): p. 1700-1715.
10. Huang, Y., et al., *Removal of indoor volatile organic compounds via photocatalytic oxidation: a short review and prospect*. Molecules, 2016. **21**(1): p. 56.
11. Greed, Z., S. Elmir, and G. Miller, *Inside Story: Indoor Air Quality*. 2004.
12. Ji, J., et al., *Mesoporous TiO₂ under VUV irradiation: Enhanced photocatalytic oxidation for VOCs degradation at room temperature*. Chemical Engineering Journal, 2017. **327**: p. 490-499.
13. Piumetti, M., D. Fino, and N. Russo, *Mesoporous manganese oxides prepared by solution combustion synthesis as catalysts for the total oxidation of VOCs*. Applied Catalysis B: Environmental, 2015. **163**: p. 277-287.
14. Zeng, M., et al., *Synergetic effect between photocatalysis on TiO₂ and thermocatalysis on CeO₂ for gas-phase oxidation of benzene on TiO₂/CeO₂ nanocomposites*. ACS Catalysis, 2015. **5**(6): p. 3278-3286.
15. Carabineiro, S., et al., *Catalytic oxidation of toluene on Ce–Co and La–Co mixed oxides synthesized by exotemplating and evaporation methods*. Catalysis Today, 2015. **244**: p. 161-171.
16. Gallegos, M.V., et al., *Removal of VOCs by catalytic process. A study of MnZnO composites synthesized from waste alkaline and Zn/C batteries*. Chemical Engineering Journal, 2017. **313**: p. 1099-1111.
17. Halepoto, A., et al., *Preparations and Characterization on Fe Based Catalyst Supported on Coconut Shell Activated Carbon CS (AC) and SCR of NO_x-HC*. Catalysis Surveys from Asia, 2020. **24**(2): p. 123-133.
18. Rescigno, R., Sacco, O., Venditto, V., Fusco, A., Donnarumma, G., Lettieri, M., ... & Vaiano, V. (2023). Photocatalytic activity of P-doped TiO₂ photocatalyst. *Photochemical & Photobiological Sciences*, 1-9.
19. Chen, X. and S.S. Mao, *Titanium dioxide nanomaterials: synthesis, properties, modifications, and applications*. Chemical reviews, 2007. **107**(7): p. 2891-2959.
20. Wen, J., Li, X., Zhang, H., Zheng, S., Yi, C., Yang, L., & Shi, J. (2023). Architecting Janus hydrogel evaporator with polydopamine-TiO₂ photocatalyst for high-efficient solar desalination and purification. *Separation and Purification Technology*, 304, 122403.
21. Zhang, Y., et al., *Nanocomposite of Ag–AgBr–TiO₂ as a photoactive and durable catalyst for degradation of volatile organic compounds in the gas phase*. Applied Catalysis B: Environmental, 2011. **106**(3-4): p. 445-452.

22. Lu, Y., et al., *The effect of activated carbon adsorption on the photocatalytic removal of formaldehyde*. Building and Environment, 2010. **45**(3): p. 615-621.
23. Suresh, S. and T.J. Bandoz, *Removal of formaldehyde on carbon-based materials: A review of the recent approaches and findings*. Carbon, 2018. **137**: p. 207-221.
24. Guo, Q., et al., *Fundamentals of TiO₂ photocatalysis: concepts, mechanisms, and challenges*. Advanced Materials, 2019. **31**(50): p. 1901997.
25. Fujishima, A., X. Zhang, and D.A. Tryk, *TiO₂ photocatalysis and related surface phenomena*. Surface science reports, 2008. **63**(12): p. 515-582.
26. Schneider, J., et al., *Understanding TiO₂ photocatalysis: mechanisms and materials*. Chemical reviews, 2014. **114**(19): p. 9919-9986.
27. Avila, P., et al., *Gas-phase photo-assisted mineralization of volatile organic compounds by monolithic titania catalysts*. Applied Catalysis B: Environmental, 1998. **17**(1-2): p. 75-88.
28. Wang, S., H. Ang, and M.O. Tade, *Volatile organic compounds in indoor environment and photocatalytic oxidation: State of the art*. Environment international, 2007. **33**(5): p. 694-705.
29. Jo, W.-K. and K.-H. Park, *Heterogeneous photocatalysis of aromatic and chlorinated volatile organic compounds (VOCs) for non-occupational indoor air application*. Chemosphere, 2004. **57**(7): p. 555-565.
30. Berenjian, A., N. Chan, and H.J. Malmiri, *Volatile organic compounds removal methods: A review*. American Journal of Biochemistry and Biotechnology, 2012. **8**(4): p. 220-229.
31. Raso, R.A., M. Zeltner, and W.J. Stark, *Indoor air purification using activated carbon adsorbers: Regeneration using catalytic combustion of intermediately stored VOC*. Industrial & Engineering Chemistry Research, 2014. **53**(49): p. 19304-19312.
32. Sahle-Demessie, E. and V.G. Devulapelli, *Oxidation of methanol and total reduced sulfur compounds with ozone over V₂O₅/TiO₂ catalyst: Effect of humidity*. Applied Catalysis A: General, 2009. **361**(1-2): p. 72-80.
33. Nuasaen, S., P. Opaprakasit, and P. Tangboriboonrat, *Hollow latex particles functionalized with chitosan for the removal of formaldehyde from indoor air*. Carbohydrate polymers, 2014. **101**: p. 179-187.
34. Boyjoo, Y., et al., *A review on photocatalysis for air treatment: From catalyst development to reactor design*. Chemical engineering journal, 2017. **310**: p. 537-559.
35. Soni, V., et al., *Abatement of formaldehyde with photocatalytic and catalytic oxidation: a review*. International Journal of Chemical Reactor Engineering, 2021. **19**(1): p. 1-29.
36. Yew, S.-P., H.-Y. Tang, and K. Sudesh, *Photocatalytic activity and biodegradation of polyhydroxybutyrate films containing titanium dioxide*. Polymer degradation and stability, 2006. **91**(8): p. 1800-1807.
37. Sreeja, S. and V. Shetty, *Microbial disinfection of water with endotoxin degradation by photocatalysis using Ag@ TiO₂ core shell nanoparticles*. Environmental Science and Pollution Research, 2016. **23**(18): p. 18154-18164.

38. Chen, J., S.-c. Kou, and C.-s. Poon, *Photocatalytic cement-based materials: Comparison of nitrogen oxides and toluene removal potentials and evaluation of self-cleaning performance*. Building and Environment, 2011. **46**(9): p. 1827-1833.
39. Ranjbari, A., et al., *Novel kinetic modeling of thiabendazole removal by adsorption and photocatalysis on porous organic polymers: Effect of pH and visible light intensity*. Chemical Engineering Journal, 2021: p. 133349.
40. ur Rehman, K., Zaman, U., Tahir, K., Khan, D., Khattak, N. S., Khan, S. U., ... & Gul, R. (2022). A *Coronopus didymus* based eco-benign synthesis of Titanium dioxide nanoparticles (TiO₂ NPs) with enhanced photocatalytic and biomedical applications. *Inorganic Chemistry Communications*, **137**, 109179.
41. Van Doorslaer, X., et al., *TiO₂ mediated heterogeneous photocatalytic degradation of moxifloxacin: operational variables and scavenger study*. Applied Catalysis B: Environmental, 2012. **111**: p. 150-156.
42. ur Rehman, K., Zaman, U., Khan, S. U., Tahir, K., Hajira, B., Al-Humaidi, J. Y., ... & Khan, D. (2023). Hydrothermal assisted eco-benign synthesis of novel β -galactosidase mediated Titanium dioxide nanoparticles (β -gal-TiO₂ NPs): Ultra efficient nanocatalyst for methylene blue degradation, inactivation of bacteria, and stabilization of DPPH radicals. *Materials Chemistry and Physics*, **294**, 126877.
43. Huang, J., et al., *Enhanced photocatalytic activity of quantum-dot-sensitized one-dimensionally-ordered ZnO nanorod photocatalyst*. Journal of Environmental Sciences, 2013. **25**(12): p. 2487-2491.
44. Elangovan, S., N. Sivakumar, and V. Chandramohan, *Magnesium doped zinc oxide nanocrystals for photo-catalytic applications*. Journal of Materials Science: Materials in Electronics, 2015. **26**(11): p. 8753-8759.
45. Kim, J., C.W. Lee, and W. Choi, *Platinized WO₃ as an environmental photocatalyst that generates OH radicals under visible light*. Environmental science & technology, 2010. **44**(17): p. 6849-6854.
46. Villa, K., et al., *Mesoporous WO₃ photocatalyst for the partial oxidation of methane to methanol using electron scavengers*. Applied Catalysis B: Environmental, 2015. **163**: p. 150-155.
47. Zhu, Z., et al., *Effect of pH on photocatalytic activity of SnO₂ microspheres via microwave solvothermal route*. Materials Research Innovations, 2014. **18**(1): p. 8-13.
48. Wang, Y., et al., *Synthesis of hollow SnO₂ microspheres and its enhanced photocatalytic properties*. Materials Letters, 2014. **137**: p. 241-244.
49. Verma, V., Al-Dossari, M., Singh, J., Rawat, M., Kordy, M. G., & Shaban, M. (2022). A review on green synthesis of TiO₂ NPs: photocatalysis and antimicrobial applications. *Polymers*, **14**(7), 1444.
50. Destailats, H., et al., *Key parameters influencing the performance of photocatalytic oxidation (PCO) air purification under realistic indoor conditions*. Applied Catalysis B: Environmental, 2012. **128**: p. 159-170.

51. Naraginti, S., et al., *Enhanced photo-catalytic activity of Sr and Ag co-doped TiO₂ nanoparticles for the degradation of Direct Green-6 and Reactive Blue-160 under UV & visible light*. Spectrochimica Acta Part A: Molecular and Biomolecular Spectroscopy, 2015. **149**: p. 571-579.
52. Pham, T.-D. and B.-K. Lee, *Selective removal of polar VOCs by novel photocatalytic activity of metals co-doped TiO₂/PU under visible light*. Chemical Engineering Journal, 2017. **307**: p. 63-73.
53. Burda, C., et al., *Chemistry and properties of nanocrystals of different shapes*. Chemical reviews, 2005. **105**(4): p. 1025-1102.
54. Li, H., et al., *Mesoporous titania spheres with tunable chamber structure and enhanced photocatalytic activity*. Journal of the American Chemical Society, 2007. **129**(27): p. 8406-8407.
55. Hosono, E., et al., *One-step synthesis of nano–micro chestnut TiO₂ with rutile nanospines on the microanatase octahedron*. Acs Nano, 2007. **1**(4): p. 273-278.
56. Macwan, D., P.N. Dave, and S. Chaturvedi, *A review on nano-TiO₂ sol–gel type syntheses and its applications*. Journal of materials science, 2011. **46**(11): p. 3669-3686.
57. Akpan, U.G. and B.H. Hameed, *Parameters affecting the photocatalytic degradation of dyes using TiO₂-based photocatalysts: a review*. Journal of hazardous materials, 2009. **170**(2-3): p. 520-529.
58. Nyamukamba, P., et al., *Synthetic methods for titanium dioxide nanoparticles: a review*. Titanium Dioxide—Material for a Sustainable Environment; Yang, D., Ed, 2018: p. 151-175.
59. Puma, G.L., et al., *Preparation of titanium dioxide photocatalyst loaded onto activated carbon support using chemical vapor deposition: a review paper*. Journal of hazardous Materials, 2008. **157**(2-3): p. 209-219.
60. Yu, H.-F., Z.-W. Zhang, and F.-C. Hu, *Phase stabilities and photocatalytic activities of P/Zn–TiO₂ nanoparticles able to operate under UV–vis light irradiation*. Journal of alloys and compounds, 2008. **465**(1-2): p. 484-490.
61. Wang, D.-H., et al., *One-step hydrothermal synthesis of N-doped TiO₂/C nanocomposites with high visible light photocatalytic activity*. Nanoscale, 2012. **4**(2): p. 576-584.
62. Mohamed, M.M. and M.S. Al-Sharif, *Visible light assisted reduction of 4-nitrophenol to 4-aminophenol on Ag/TiO₂ photocatalysts synthesized by hybrid templates*. Applied Catalysis B: Environmental, 2013. **142**: p. 432-441.
63. Zuo, G.-M., et al., *Study on photocatalytic degradation of several volatile organic compounds*. Journal of hazardous materials, 2006. **128**(2-3): p. 158-163.
64. Watson, S.S., et al., *The effect of preparation method on the photoactivity of crystalline titanium dioxide particles*. Chemical Engineering Journal, 2003. **95**(1-3): p. 213-220.

65. Wang, W.-K., et al., *Self-induced synthesis of phase-junction TiO₂ with a tailored rutile to anatase ratio below phase transition temperature*. Scientific reports, 2016. **6**(1): p. 1-10.
66. Pelaez, M., et al., *A review on the visible light active titanium dioxide photocatalysts for environmental applications*. Applied Catalysis B: Environmental, 2012. **125**: p. 331-349.
67. Porkodi, K. and S.D. Arokiamary, *Synthesis and spectroscopic characterization of nanostructured anatase titania: A photocatalyst*. Materials Characterization, 2007. **58**(6): p. 495-503.
68. Lin, L., et al., *Photocatalytic oxidation for degradation of VOCs*. 2013.
69. Hernández-Alonso, M.D., et al., *Development of alternative photocatalysts to TiO₂: challenges and opportunities*. Energy & Environmental Science, 2009. **2**(12): p. 1231-1257.
70. Nah, Y.C., I. Paramasivam, and P. Schmuki, *Doped TiO₂ and TiO₂ nanotubes: synthesis and applications*. ChemPhysChem, 2010. **11**(13): p. 2698-2713.
71. Likodimos, V., et al., *Phase composition, size, orientation, and antenna effects of self-assembled anodized titania nanotube arrays: A polarized micro-Raman investigation*. The Journal of Physical Chemistry C, 2008. **112**(33): p. 12687-12696.
72. Kontos, A., et al., *Photo-induced effects on self-organized TiO₂ nanotube arrays: the influence of surface morphology*. Nanotechnology, 2008. **20**(4): p. 045603.
73. Nguyen-Phan, T.-D. and E.W. Shin, *Morphological effect of TiO₂ catalysts on photocatalytic degradation of methylene blue*. Journal of industrial and engineering Chemistry, 2011. **17**(3): p. 397-400.
74. D'Arienzo, M., et al., *Photogenerated defects in shape-controlled TiO₂ anatase nanocrystals: a probe to evaluate the role of crystal facets in photocatalytic processes*. Journal of the American Chemical Society, 2011. **133**(44): p. 17652-17661.
75. Pastrana-Martinez, L.M., et al., *Advanced nanostructured photocatalysts based on reduced graphene oxide-TiO₂ composites for degradation of diphenhydramine pharmaceutical and methyl orange dye*. Applied Catalysis B: Environmental, 2012. **123**: p. 241-256.
76. Choi, J., H. Park, and M.R. Hoffmann, *Effects of single metal-ion doping on the visible-light photoreactivity of TiO₂*. The Journal of Physical Chemistry C, 2010. **114**(2): p. 783-792.
77. Yu, J., Q. Xiang, and M. Zhou, *Preparation, characterization and visible-light-driven photocatalytic activity of Fe-doped titania nanorods and first-principles study for electronic structures*. Applied Catalysis B: Environmental, 2009. **90**(3-4): p. 595-602.
78. Asahi, R., et al., *Visible-light photocatalysis in nitrogen-doped titanium oxides*. science, 2001. **293**(5528): p. 269-271.
79. Yu, J., G. Dai, and B. Huang, *Fabrication and characterization of visible-light-driven plasmonic photocatalyst Ag/AgCl/TiO₂ nanotube arrays*. The Journal of Physical Chemistry C, 2009. **113**(37): p. 16394-16401.

80. Wang, C., et al., *Visible light photoreduction of CO₂ using CdSe/Pt/TiO₂ heterostructured catalysts*. The Journal of Physical Chemistry Letters, 2010. **1**(1): p. 48-53.
81. Wang, Z., et al., *Crystal facets controlled synthesis of graphene@ TiO₂ nanocomposites by a one-pot hydrothermal process*. CrystEngComm, 2012. **14**(5): p. 1687-1692.
82. Li, L., G.S. Rohrer, and P.A. Salvador, *Heterostructured ceramic powders for photocatalytic hydrogen production: nanostructured TiO₂ shells surrounding microcrystalline (Ba, Sr) TiO₃ cores*. Journal of the American Ceramic Society, 2012. **95**(4): p. 1414-1420.
83. Han, X., et al., *Carbonate ions-assisted syntheses of anatase TiO₂ nanoparticles exposed with high energy {001} facets*. Rsc Advances, 2012. **2**(8): p. 3251-3253.
84. Selçuk, S. and A. Selloni, *Surface structure and reactivity of anatase TiO₂ crystals with dominant {001} facets*. The Journal of Physical Chemistry C, 2013. **117**(12): p. 6358-6362.
85. Liu, B. and E.S. Aydil, *Anatase TiO₂ films with reactive {001} facets on transparent conductive substrate*. Chemical Communications, 2011. **47**(33): p. 9507-9509.
86. Chen, J.S., et al., *Constructing hierarchical spheres from large ultrathin anatase TiO₂ nanosheets with nearly 100% exposed {001} facets for fast reversible lithium storage*. Journal of the American Chemical Society, 2010. **132**(17): p. 6124-6130.
87. Lai, Z., et al., *Low temperature solvothermal synthesis of anatase TiO₂ single crystals with wholly {100} and {001} faceted surfaces*. Journal of Materials Chemistry, 2012. **22**(45): p. 23906-23912.
88. Selloni, A., *Anatase shows its reactive side*. Nature Materials, 2008. **7**(8): p. 613-615.
89. Wang, J., et al., *Ordered mesoporous TiO₂ with exposed {001} facets and enhanced activity in photocatalytic selective oxidation of alcohols*. Journal of Materials Chemistry A, 2013. **1**(4): p. 1296-1302.
90. Ye, L., et al., *Synthesis of anatase TiO₂ nanocrystals with {101}, {001} or {010} single facets of 90% level exposure and liquid-phase photocatalytic reduction and oxidation activity orders*. Journal of Materials Chemistry A, 2013. **1**(35): p. 10532-10537.
91. Sofianou, M.-V., et al., *Study of TiO₂ anatase nano and microstructures with dominant {001} facets for NO oxidation*. Environmental Science and Pollution Research, 2012. **19**(9): p. 3719-3726.
92. Sun, L., et al., *Anatase TiO₂ nanocrystals with exposed {001} facets on graphene sheets via molecular grafting for enhanced photocatalytic activity*. Nanoscale, 2012. **4**(2): p. 613-620.
93. Xu, H., et al., *High-active anatase TiO₂ nanosheets exposed with 95%{100} facets toward efficient H₂ evolution and CO₂ photoreduction*. ACS applied materials & interfaces, 2013. **5**(4): p. 1348-1354.
94. Yu, J., et al., *Fabrication and enhanced visible-light photocatalytic activity of carbon self-doped TiO₂ sheets with exposed {001} facets*. Journal of Materials Chemistry, 2011. **21**(4): p. 1049-1057.

95. Xiang, Q., J. Yu, and M. Jaroniec, *Nitrogen and sulfur co-doped TiO₂ nanosheets with exposed {001} facets: synthesis, characterization and visible-light photocatalytic activity*. *Physical Chemistry Chemical Physics*, 2011. **13**(11): p. 4853-4861.
96. Zhang, Y., C. Li, and C. Pan, *N+ Ni Codoped Anatase TiO₂ Nanocrystals with Exposed {001} Facets Through Two-Step Hydrothermal Route*. *Journal of the American Ceramic Society*, 2012. **95**(9): p. 2951-2956.
97. Zhang, J., J. Xi, and Z. Ji, *Mo+ N codoped TiO₂ sheets with dominant {001} facets for enhancing visible-light photocatalytic activity*. *Journal of Materials Chemistry*, 2012. **22**(34): p. 17700-17708.
98. Yu, J., L. Qi, and M. Jaroniec, *Hydrogen production by photocatalytic water splitting over Pt/TiO₂ nanosheets with exposed (001) facets*. *The Journal of Physical Chemistry C*, 2010. **114**(30): p. 13118-13125.
99. Zhu, S., et al., *Effect of Au supported TiO₂ with dominant exposed {0 0 1} facets on the visible-light photocatalytic activity*. *Applied Catalysis B: Environmental*, 2012. **119**: p. 146-155.
100. Wen, C.Z., et al., *Synthesis of high-reactive facets dominated anatase TiO₂*. *Journal of Materials Chemistry*, 2011. **21**(20): p. 7052-7061.
101. Liu, S., J. Yu, and M. Jaroniec, *Anatase TiO₂ with dominant high-energy {001} facets: synthesis, properties, and applications*. *Chemistry of Materials*, 2011. **23**(18): p. 4085-4093.
102. Thevenet, F., C. Guillard, and A. Rousseau, *Acetylene photocatalytic oxidation using continuous flow reactor: Gas phase and adsorbed phase investigation, assessment of the photocatalyst deactivation*. *Chemical Engineering Journal*, 2014. **244**: p. 50-58.
103. Monteiro, R.A., et al., *Gas phase oxidation of n-decane and PCE by photocatalysis using an annular photoreactor packed with a monolithic catalytic bed coated with P25 and PC500*. *Applied Catalysis B: Environmental*, 2015. **165**: p. 306-315.
104. Andryushina, N.S. and O.L. Stroyuk, *Influence of colloidal graphene oxide on photocatalytic activity of nanocrystalline TiO₂ in gas-phase ethanol and benzene oxidation*. *Applied Catalysis B: Environmental*, 2014. **148**: p. 543-549.
105. Tejasvi, R., M. Sharma, and K. Upadhyay, *Passive photo-catalytic destruction of air-borne VOCs in high traffic areas using TiO₂-coated flexible PVC sheet*. *Chemical Engineering Journal*, 2015. **262**: p. 875-881.
106. Hou, W.-M. and Y. Ku, *Photocatalytic decomposition of gaseous isopropanol in a tubular optical fiber reactor under periodic UV-LED illumination*. *Journal of Molecular Catalysis A: Chemical*, 2013. **374**: p. 7-11.
107. Xie, H., B. Liu, and X. Zhao, *Facile process to greatly improve the photocatalytic activity of the TiO₂ thin film on window glass for the photodegradation of acetone and benzene*. *Chemical Engineering Journal*, 2016. **284**: p. 1156-1164.
108. Antonello, A., et al., *Photocatalytic remediation of indoor pollution by transparent TiO₂ films*. *Catalysis today*, 2014. **230**: p. 35-40.

109. Bianchi, C., et al., *Photocatalytic degradation of acetone, acetaldehyde and toluene in gas-phase: comparison between nano and micro-sized TiO₂*. Applied Catalysis B: Environmental, 2014. **146**: p. 123-130.
110. Le Béhec, M., et al., *Comparison of kinetics of acetone, heptane and toluene photocatalytic mineralization over TiO₂ microfibers and Quartzel® mats*. Applied Catalysis B: Environmental, 2015. **179**: p. 78-87.
111. He, F., et al., *Solvothermal synthesis of mesoporous TiO₂: The effect of morphology, size and calcination progress on photocatalytic activity in the degradation of gaseous benzene*. Chemical Engineering Journal, 2014. **237**: p. 312-321.
112. Ren, L., et al., *The pivotal effect of the interaction between reactant and anatase TiO₂ nanosheets with exposed {0 0 1} facets on photocatalysis for the photocatalytic purification of VOCs*. Applied Catalysis B: Environmental, 2016. **181**: p. 625-634.
113. Liu, Z., et al., *Study of adsorption-assisted photocatalytic oxidation of benzene with TiO₂/SiO₂ nanocomposites*. Applied Catalysis A: General, 2013. **451**: p. 120-126.
114. Banisharif, A., et al., *Highly active Fe₂O₃-doped TiO₂ photocatalyst for degradation of trichloroethylene in air under UV and visible light irradiation: experimental and computational studies*. Applied Catalysis B: Environmental, 2015. **165**: p. 209-221.
115. Huang, H., et al., *Enhanced degradation of gaseous benzene under vacuum ultraviolet (VUV) irradiation over TiO₂ modified by transition metals*. Chemical Engineering Journal, 2015. **259**: p. 534-541.
116. Vargas, D.X.M., et al., *Photocatalytic degradation of trichloroethylene in a continuous annular reactor using Cu-doped TiO₂ catalysts by sol-gel synthesis*. Applied Catalysis B: Environmental, 2015. **179**: p. 249-261.
117. Zhuang, H., et al., *Visible light-driven decomposition of gaseous benzene on robust Sn²⁺-doped anatase TiO₂ nanoparticles*. Rsc Advances, 2014. **4**(65): p. 34315-34324.
118. Murcia, J., et al., *Cyclohexane photocatalytic oxidation on Pt/TiO₂ catalysts*. Catalysis today, 2013. **209**: p. 164-169.
119. Chen, Y., et al., *A facile approach to synthesize N-doped and oxygen-deficient TiO₂ with high visible-light activity for benzene decomposition*. Materials Letters, 2013. **94**: p. 154-157.
120. Han, Z., et al., *Experimental study on visible-light induced photocatalytic oxidation of gaseous formaldehyde by polyester fiber supported photocatalysts*. Chemical engineering journal, 2013. **218**: p. 9-18.
121. Ong, W.-J., et al., *Highly reactive {001} facets of TiO₂-based composites: synthesis, formation mechanism and characterization*. Nanoscale, 2014. **6**(4): p. 1946-2008.
122. Yang, J., et al., *Roles of cocatalysts in photocatalysis and photoelectrocatalysis*. Accounts of chemical research, 2013. **46**(8): p. 1900-1909.
123. Wang, G., Y. Ling, and Y. Li, *Oxygen-deficient metal oxide nanostructures for photoelectrochemical water oxidation and other applications*. Nanoscale, 2012. **4**(21): p. 6682-6691.

124. Lv, Y., Y. Zhu, and Y. Zhu, *Enhanced photocatalytic performance for the BiPO₄-x nanorod induced by surface oxygen vacancy*. The Journal of Physical Chemistry C, 2013. **117**(36): p. 18520-18528.
125. Bai, X., et al., *Performance enhancement of ZnO photocatalyst via synergic effect of surface oxygen defect and graphene hybridization*. Langmuir, 2013. **29**(9): p. 3097-3105.
126. Ni, C., et al., *Synergistic role of electron-trapped oxygen vacancy and exposed TiO₂ [0 0 1] facets toward electrochemical p-nitrophenol reduction: Characterization, performance and mechanism*. Chemical Engineering Journal, 2021. **411**: p. 128485.
127. Chen, X., et al., *Increasing solar absorption for photocatalysis with black hydrogenated titanium dioxide nanocrystals*. Science, 2011. **331**(6018): p. 746-750.
128. Chen, X., L. Liu, and F. Huang, *Black titanium dioxide (TiO₂) nanomaterials*. Chemical Society Reviews, 2015. **44**(7): p. 1861-1885.
129. Xia, T. and X. Chen, *Revealing the structural properties of hydrogenated black TiO₂ nanocrystals*. Journal of Materials Chemistry A, 2013. **1**(9): p. 2983-2989.
130. Liu, L., et al., *Hydrogenation and disorder in engineered black TiO₂*. Physical review letters, 2013. **111**(6): p. 065505.
131. Qiu, J., et al., *Blue hydrogenated lithium titanate as a high-rate anode material for lithium-ion batteries*. Journal of Materials Chemistry A, 2014. **2**(18): p. 6353-6358.
132. Zhu, G., et al., *Hydrogenated blue titania with high solar absorption and greatly improved photocatalysis*. Nanoscale, 2016. **8**(8): p. 4705-4712.
133. Zou, X., et al., *Facile synthesis of thermal-and photostable titania with paramagnetic oxygen vacancies for visible-light photocatalysis*. Chemistry—A European Journal, 2013. **19**(8): p. 2866-2873.
134. Huo, J., et al., *In situ surface hydrogenation synthesis of Ti³⁺ self-doped TiO₂ with enhanced visible light photoactivity*. Nanoscale, 2014. **6**(15): p. 9078-9084.
135. Cai, J., et al., *In situ formation of disorder-engineered TiO₂ (B)-anatase heterophase junction for enhanced photocatalytic hydrogen evolution*. ACS applied materials & interfaces, 2015. **7**(45): p. 24987-24992.
136. Fujishima, A. and K. Honda, *Electrochemical photolysis of water at a semiconductor electrode*. nature, 1972. **238**(5358): p. 37-38.
137. Feng, C., et al., *Coaction of sub-band and doped nitrogen on visible light photoactivity of N-doped TiO₂*. Photochemistry and photobiology, 2010. **86**(6): p. 1222-1229.
138. Qian, L., et al., *Study of the visible-excitation luminescence of NTA-TiO₂ (AB) with single-electron-trapped oxygen vacancies*. Applied Physics A, 2005. **80**(8): p. 1801-1805.
139. Chen, W., et al., *TEM study on the formation mechanism of sodium titanate nanotubes*. Journal of Nanoparticle Research, 2007. **9**(6): p. 1173-1180.
140. Li, Q., et al., *Photo and photoelectrochemical properties of p-type low-temperature dehydrated nanotube titanate acid*. Electrochemistry communications, 2006. **8**(5): p. 741-746.

141. Ihara, T., et al., *Preparation of a visible-light-active TiO₂ photocatalyst by RF plasma treatment*. Journal of materials science, 2001. **36**(17): p. 4201-4207.
142. Li, W., et al., *Electron transport mechanism of tungsten trioxide powder thin film studied by investigating effect of annealing on resistivity*. Microelectronics Reliability, 2015. **55**(2): p. 407-410.
143. Gordon, T.R., et al., *Nonaqueous synthesis of TiO₂ nanocrystals using TiF₄ to engineer morphology, oxygen vacancy concentration, and photocatalytic activity*. Journal of the American Chemical Society, 2012. **134**(15): p. 6751-6761.
144. Zuo, F., et al., *Self-doped Ti³⁺ enhanced photocatalyst for hydrogen production under visible light*. Journal of the American Chemical Society, 2010. **132**(34): p. 11856-11857.
145. Fukushi, D., et al., *Effect of oxygen vacancy in tungsten oxide on the photocatalytic activity for decomposition of organic materials in the gas phase*. Microelectronics Reliability, 2017. **79**: p. 1-4.
146. Shockley, W. and W. Read Jr, *Statistics of the recombinations of holes and electrons*. Physical review, 1952. **87**(5): p. 835.
147. Hall, R.N., *Electron-hole recombination in germanium*. Physical review, 1952. **87**(2): p. 387.
148. Kang, X., et al., *Titanium dioxide: from engineering to applications*. Catalysts, 2019. **9**(2): p. 191.
149. Li, J., et al., *Synergistic effect of surface and bulk single-electron-trapped oxygen vacancy of TiO₂ in the photocatalytic reduction of CO₂*. Applied Catalysis B: Environmental, 2017. **206**: p. 300-307.
150. Liu, Y., et al., *TiO₂/Cu₂O core/ultrathin shell nanorods as efficient and stable photocatalysts for water reduction*. Angewandte Chemie, 2015. **127**(50): p. 15475-15480.
151. An, X., et al., *Oxygen vacancy mediated construction of anatase/brookite heterophase junctions for high-efficiency photocatalytic hydrogen evolution*. Journal of Materials Chemistry A, 2017. **5**(47): p. 24989-24994.
152. Comparelli, R., et al., *Photocatalytic degradation of azo dyes by organic-capped anatase TiO₂ nanocrystals immobilized onto substrates*. Applied Catalysis B: Environmental, 2005. **55**(2): p. 81-91.
153. Hufschmidt, D., et al., *Photocatalytic water treatment: fundamental knowledge required for its practical application*. Water Science and Technology, 2004. **49**(4): p. 135-140.
154. Agrios, A.G. and P. Pichat, *State of the art and perspectives on materials and applications of photocatalysis over TiO₂*. Journal of Applied Electrochemistry, 2005. **35**(7-8): p. 655-663.
155. Formenti, M., et al., *Heterogeneous photocatalysis for partial oxidation of paraffins*. Chemical technology, 1971(NNOV): p. 680-+.
156. Bickley, R. and F. Stone, *Photoadsorption and photocatalysis at rutile surfaces: I. Photoadsorption of oxygen*. Journal of Catalysis, 1973. **31**(3): p. 389-397.

157. Bickley, R., G. Munuera, and F. Stone, *Photoadsorption and photocatalysis at rutile surfaces: II. Photocatalytic oxidation of isopropanol*. Journal of Catalysis, 1973. **31**(3): p. 398-407.
158. Sun, H., et al., *Room-light-induced indoor air purification using an efficient Pt/N-TiO₂ photocatalyst*. Applied Catalysis B: Environmental, 2011. **108**: p. 127-133.
159. Yu, W., et al., *Formation of formaldehyde and other byproducts by TiO₂ photocatalyst materials*. Sustainability, 2021. **13**(9): p. 4821.
160. Peral, J. and D.F. Ollis, *Heterogeneous photocatalytic oxidation of gas-phase organics for air purification: acetone, 1-butanol, butyraldehyde, formaldehyde, and m-xylene oxidation*. Journal of Catalysis, 1992. **136**(2): p. 554-565.
161. Mahmood, A., et al., *Degradation behavior of mixed and isolated aromatic ring containing VOCs: Langmuir-Hinshelwood kinetics, photodegradation, in-situ FTIR and DFT studies*. Journal of Environmental Chemical Engineering, 2021. **9**(2): p. 105069.
162. Elfalleh, W., et al., *Innovative and stable TiO₂ supported catalytic surfaces removing aldehydes under UV-light irradiation*. Journal of Photochemistry and Photobiology A: Chemistry, 2017. **343**: p. 96-102.
163. Shi, T., et al., *H₂O-involved two-electron pathway for photooxidation of aldehydes on TiO₂: an isotope labeling study*. Environmental science & technology, 2015. **49**(5): p. 3024-3031.
164. Sun, H. and S. Wang, *Research advances in the synthesis of nanocarbon-based photocatalysts and their applications for photocatalytic conversion of carbon dioxide to hydrocarbon fuels*. Energy & fuels, 2014. **28**(1): p. 22-36.
165. Zhou, L., et al., *Construction of quantum-scale catalytic regions on anatase TiO₂ nanoparticles by loading TiO₂ quantum dots for the photocatalytic degradation of VOCs*. Ceramics International, 2021.
166. Quici, N., et al., *Effect of key parameters on the photocatalytic oxidation of toluene at low concentrations in air under 254+ 185 nm UV irradiation*. Applied Catalysis B: Environmental, 2010. **95**(3-4): p. 312-319.
167. Zhong, L., et al., *Experimental and modeling study of visible light responsive photocatalytic oxidation (PCO) materials for toluene degradation*. Applied Catalysis B: Environmental, 2017. **216**: p. 122-132.
168. Weon, S., J. Kim, and W. Choi, *Dual-components modified TiO₂ with Pt and fluoride as deactivation-resistant photocatalyst for the degradation of volatile organic compound*. Applied Catalysis B: Environmental, 2018. **220**: p. 1-8.
169. Huang, J., et al., *Degradation of benzene over a zinc germanate photocatalyst under ambient conditions*. Environmental science & technology, 2008. **42**(19): p. 7387-7391.
170. Wang, W. and Y. Ku, *Photocatalytic degradation of gaseous benzene in air streams by using an optical fiber photoreactor*. Journal of Photochemistry and Photobiology A: Chemistry, 2003. **159**(1): p. 47-59.

171. Puddu, V., et al., *TiO₂ photocatalyst for indoor air remediation: Influence of crystallinity, crystal phase, and UV radiation intensity on trichloroethylene degradation*. Applied Catalysis B: Environmental, 2010. **94**(3-4): p. 211-218.
172. Seyama, T., et al., *Photocatalytic degradation of trichloroethylene on platinum ion-doped TiO₂ under visible light irradiation*. Research on Chemical Intermediates, 2017. **43**(9): p. 5025-5039.
173. Ou, H.-H. and S.-L. Lo, *Photocatalysis of gaseous trichloroethylene (TCE) over TiO₂: The effect of oxygen and relative humidity on the generation of dichloroacetyl chloride (DCAC) and phosgene*. Journal of hazardous materials, 2007. **146**(1-2): p. 302-308.
174. Szatmáry, L., et al., *Low-temperature deposition of anatase on nanofiber materials for photocatalytic NO_x removal*. Catalysis Today, 2014. **230**: p. 74-78.
175. Wang, C., et al., *The effects of Mn²⁺ precursors on the structure and ozone decomposition activity of cryptomelane-type manganese oxide (OMS-2) catalysts*. The Journal of Physical Chemistry C, 2015. **119**(40): p. 23119-23126.
176. Ma, J., H. He, and F. Liu, *Effect of Fe on the photocatalytic removal of NO_x over visible light responsive Fe/TiO₂ catalysts*. Applied Catalysis B: Environmental, 2015. **179**: p. 21-28.
177. Nguyen, N.H., H.-Y. Wu, and H. Bai, *Photocatalytic reduction of NO₂ and CO₂ using molybdenum-doped titania nanotubes*. Chemical Engineering Journal, 2015. **269**: p. 60-66.
178. Hu, Y., et al., *Enhanced photocatalytic activity of Pt-doped TiO₂ for NO_x oxidation both under UV and visible light irradiation: a synergistic effect of lattice Pt⁴⁺ and surface PtO*. Chemical Engineering Journal, 2015. **274**: p. 102-112.
179. Zhu, W., et al., *Highly efficient and stable Au/CeO₂-TiO₂ photocatalyst for nitric oxide abatement: potential application in flue gas treatment*. Langmuir, 2015. **31**(39): p. 10822-10830.
180. Seifvand, N. and E. Kowsari, *Novel TiO₂/graphene oxide functionalized with a cobalt complex for significant degradation of NO_x and CO*. RSC advances, 2015. **5**(114): p. 93706-93716.
181. Alonso-Tellez, A., et al., *H₂S photocatalytic oxidation over WO₃/TiO₂ Hombikat UV100*. Environmental Science and Pollution Research, 2014. **21**(5): p. 3503-3514.
182. Jiao, Y., H. Jiang, and F. Chen, *RuO₂/TiO₂/Pt ternary photocatalysts with epitaxial heterojunction and their application in CO oxidation*. Acs Catalysis, 2014. **4**(7): p. 2249-2257.
183. Liu, H., X. Yu, and H. Yang, *The integrated photocatalytic removal of SO₂ and NO using Cu doped titanium dioxide supported by multi-walled carbon nanotubes*. Chemical Engineering Journal, 2014. **243**: p. 465-472.
184. Yamamoto, A., et al., *Visible-light-assisted selective catalytic reduction of nitric oxide with ammonia over dye-modified titania photocatalysts*. ChemCatChem, 2015. **7**(12): p. 1818-1825.

185. Kashif, M., et al., *Fully selective catalytic oxidation of NO to NO₂ over most active Ga-PCH catalyst*. Journal of Environmental Chemical Engineering, 2020. **8**(2): p. 103524.
186. Ângelo, J., et al., *An overview of photocatalysis phenomena applied to NO_x abatement*. Journal of environmental management, 2013. **129**: p. 522-539.
187. Kashif, M., et al., *Most efficient mesoporous Mn/Ga-PCH catalyst for low-temperature selective catalytic reduction of NO with C₃H₆*. Vacuum, 2022: p. 110879.
188. Khan, M.N., et al., *SO₂-tolerant NO_x reduction over ceria-based catalysts: Shielding effects of hollandite Mn-Ti oxides*. Chemical Engineering Journal, 2020. **397**: p. 125535.
189. Luévano-Hipólito, E., et al., *Precipitation synthesis of WO₃ for NO_x removal using PEG as template*. Ceramics International, 2014. **40**(8): p. 12123-12128.
190. Luevano-Hipolito, E., et al., *Synthesis, characterization and photocatalytic activity of WO₃/TiO₂ for NO removal under UV and visible light irradiation*. Materials Chemistry and Physics, 2014. **148**(1-2): p. 208-213.
191. Mendoza, J.A., D.H. Lee, and J.-H. Kang, *Photocatalytic removal of gaseous nitrogen oxides using WO₃/TiO₂ particles under visible light irradiation: Effect of surface modification*. Chemosphere, 2017. **182**: p. 539-546.
192. Ma, J., et al., *Photocatalytic Removal of NO_x over Visible Light Responsive Oxygen-Deficient TiO₂*. The Journal of Physical Chemistry C, 2014. **118**(14): p. 7434-7441.
193. Bastida, M.A.C., et al., *Sodium Titanate Synthesis For The Photocatalytic Degradation of NO*. 2021.
194. Wang, L., Y. Zhao, and J. Zhang, *Photochemical removal of SO₂ over TiO₂-based nanofibers by a dry photocatalytic oxidation process*. Energy & Fuels, 2017. **31**(9): p. 9905-9914.
195. Fernandes, C.N., et al., *Using TiO₂ nanoparticles as a SO₂ catalyst in cement mortars*. Construction And Building Materials, 2020. **257**: p. 119542.
196. Topalian, Z., et al., *Spectroscopic study of the photofixation of SO₂ on anatase TiO₂ thin films and their oleophobic properties*. ACS applied materials & interfaces, 2012. **4**(2): p. 672-679.
197. Xia, D., et al., *Simultaneous photocatalytic elimination of gaseous NO and SO₂ in a BiOI/Al₂O₃-padded trickling scrubber under visible light*. Chemical Engineering Journal, 2015. **279**: p. 929-938.
198. Hassan, H.M., et al., *A comparative study of the incorporation of TiO₂ into MCM-41 nanostructure via different approaches and its effect on the photocatalytic degradation of methylene blue and CO oxidation*. Reaction Kinetics, Mechanisms and Catalysis, 2017. **120**(2): p. 791-807.
199. Lu, Y., et al., *Feasibility analysis on photocatalytic removal of gaseous ozone in aircraft cabins*. Building and Environment, 2014. **81**: p. 42-50.
200. Nishimura, A., et al., *Using TiO₂ photocatalyst with adsorbent to oxidize carbon monoxide in rich hydrogen*. Catalysis Today, 2010. **158**(3-4): p. 296-304.

201. Liu, G., et al., *Efficient degradation of H₂S over transition metal modified TiO₂ under VUV irradiation: Performance and mechanism*. Applied Surface Science, 2018. **433**: p. 329-335.
202. Sheng, H., et al., *Urchin-inspired TiO₂@ MIL-101 double-shell hollow particles: adsorption and highly efficient photocatalytic degradation of hydrogen sulfide*. Chemistry of Materials, 2017. **29**(13): p. 5612-5616.
203. Shahzad, N. and R.W. Azfar, *Comparison of H₂S gas destruction potential using TiO₂ nanofibers and nanoparticles*. Environmental Science and Pollution Research, 2017. **24**(2): p. 1133-1136.
204. Bhirud, A.P., et al., *In-situ preparation of N-TiO₂/graphene nanocomposite and its enhanced photocatalytic hydrogen production by H₂S splitting under solar light*. Nanoscale, 2015. **7**(11): p. 5023-5034.
205. Islam, A., et al., *Sensitization of nanocrystalline TiO₂ film by ruthenium (II) diimine dithiolate complexes*. Journal of Photochemistry and Photobiology A: Chemistry, 2001. **145**(1-2): p. 135-141.
206. O'Regan, B. and M. Grätzel, *Nature*1991, 353, 737. Google Scholar There is no corresponding record for this reference.
207. Borgarello, E., et al., *Visible light induced water cleavage in colloidal solutions of chromium-doped titanium dioxide particles*. Journal of the American Chemical Society, 1982. **104**(11): p. 2996-3002.
208. Hoffmann, M.R., et al., *Environmental applications of semiconductor photocatalysis*. Chemical reviews, 1995. **95**(1): p. 69-96.
209. Anpo, M., *Preparation, characterization, and reactivities of highly functional titanium oxide-based photocatalysts able to operate under UV-visible light irradiation: approaches in realizing high efficiency in the use of visible light*. Bulletin of the Chemical Society of Japan, 2004. **77**(8): p. 1427-1442.
210. Murakami, N., et al., *Development of a visible-light-responsive rutile rod by site-selective modification of iron (III) ion on {1 1 1} exposed crystal faces*. Applied Catalysis B: Environmental, 2010. **97**(1-2): p. 115-119.
211. Choi, W., A. Termin, and M.R. Hoffmann, *The role of metal ion dopants in quantum-sized TiO₂: correlation between photoreactivity and charge carrier recombination dynamics*. The Journal of Physical Chemistry, 2002. **98**(51): p. 13669-13679.
212. Kang, M., *The superhydrophilicity of Al-TiO₂ nanometer sized material synthesized using a solvothermal method*. Materials Letters, 2005. **59**(24-25): p. 3122-3127.
213. Morikawa, T., Y. Irokawa, and T. Ohwaki, *Enhanced photocatalytic activity of TiO₂- xNx loaded with copper ions under visible light irradiation*. Applied Catalysis A: General, 2006. **314**(1): p. 123-127.
214. Choi, W., A. Termin, and M.R. Hoffmann, *Effects of metal-ion dopants on the photocatalytic reactivity of quantum-sized TiO₂ particles*. Angewandte Chemie International Edition in English, 1994. **33**(10): p. 1091-1092.

215. Yan, N., et al., *Preparation and properties of ce-doped TiO₂ photocatalyst*. Materials Research Bulletin, 2012. **47**(8): p. 1869-1873.
216. Zhu, J., et al., *Fe³⁺-TiO₂ photocatalysts prepared by combining sol-gel method with hydrothermal treatment and their characterization*. Journal of Photochemistry and Photobiology A: Chemistry, 2006. **180**(1-2): p. 196-204.
217. Zhu, J., et al., *Hydrothermal doping method for preparation of Cr³⁺-TiO₂ photocatalysts with concentration gradient distribution of Cr³⁺*. Applied Catalysis B: Environmental, 2006. **62**(3-4): p. 329-335.
218. Tian, B., et al., *Flame sprayed V-doped TiO₂ nanoparticles with enhanced photocatalytic activity under visible light irradiation*. Chemical Engineering Journal, 2009. **151**(1-3): p. 220-227.
219. Lin, W.-C. and Y.-J. Lin, *Effect of vanadium (IV)-doping on the visible light-induced catalytic activity of titanium dioxide catalysts for methylene blue degradation*. Environmental engineering science, 2012. **29**(6): p. 447-452.
220. Jaiswal, R., et al., *Improved visible light photocatalytic activity of TiO₂ co-doped with Vanadium and Nitrogen*. Applied Catalysis B: Environmental, 2012. **126**: p. 47-54.
221. Linsebigler, A.L., G. Lu, and J.T. Yates Jr, *Photocatalysis on TiO₂ surfaces: principles, mechanisms, and selected results*. Chemical reviews, 1995. **95**(3): p. 735-758.
222. Kim, S., S.-J. Hwang, and W. Choi, *Visible light active platinum-ion-doped TiO₂ photocatalyst*. The Journal of Physical Chemistry B, 2005. **109**(51): p. 24260-24267.
223. Wang, F., et al., *Analysis of the promoted activity and molecular mechanism of hydrogen production over fine Au-Pt alloyed TiO₂ photocatalysts*. ACS Catalysis, 2015. **5**(7): p. 3924-3931.
224. Choi, Y., et al., *Sequential process combination of photocatalytic oxidation and dark reduction for the removal of organic pollutants and Cr (VI) using Ag/TiO₂*. Environmental science & technology, 2017. **51**(7): p. 3973-3981.
225. Karmaoui, M., et al., *Modification of anatase using noble-metals (Au, Pt, Ag): Toward a nanoheterojunction exhibiting simultaneously photocatalytic activity and plasmonic gas sensing*. Applied Catalysis B: Environmental, 2017. **218**: p. 370-384.
226. Zhao, Y., et al., *Solvothermal preparation of Sn⁴⁺ doped anatase TiO₂ nanocrystals from peroxo-metal-complex and their photocatalytic activity*. Applied Catalysis B: Environmental, 2011. **103**(3-4): p. 436-443.
227. Sun, L., et al., *Synergistic effects in La/N codoped TiO₂ anatase (101) surface correlated with enhanced visible-light photocatalytic activity*. Langmuir, 2012. **28**(13): p. 5882-5891.
228. Xing, M.Y., et al., *One-step hydrothermal method to prepare carbon and lanthanum co-doped TiO₂ nanocrystals with exposed {001} facets and their high UV and visible-light photocatalytic activity*. Chemistry—A European Journal, 2011. **17**(41): p. 11432-11436.
229. Ma, Y., et al., *Synthesis of well ordered mesoporous Yb, N co-doped TiO₂ with superior visible photocatalytic activity*. Microporous and mesoporous materials, 2012. **156**: p. 145-152.

230. Anandan, S., Y. Ikuma, and V. Murugesan, *Highly active rare-earth-metal La-doped photocatalysts: fabrication, characterization, and their photocatalytic activity*. International Journal of Photoenergy, 2011. **2012**.
231. Parida, K. and N. Sahu, *Visible light induced photocatalytic activity of rare earth titania nanocomposites*. Journal of Molecular Catalysis A: Chemical, 2008. **287**(1-2): p. 151-158.
232. El-Bahy, Z.M., A.A. Ismail, and R.M. Mohamed, *Enhancement of titania by doping rare earth for photodegradation of organic dye (Direct Blue)*. Journal of Hazardous Materials, 2009. **166**(1): p. 138-143.
233. Baiju, K., et al., *Mesoporous gadolinium doped titania photocatalyst through an aqueous sol-gel method*. Journal of Alloys and Compounds, 2010. **505**(1): p. 194-200.
234. Anpo, M., et al., *Photoformation and structure of oxygen anion radicals (O₂⁻) and nitrogen-containing anion radicals adsorbed on highly dispersed titanium oxide anchored onto porous Vycor glass*. The Journal of Physical Chemistry, 1985. **89**(26): p. 5689-5694.
235. Gritscov, A., V. Shvets, and V. Kazansky, *A luminescence study of the photoreduction of vanadium (V) supported on silica gel*. Chemical Physics Letters, 1975. **35**(4): p. 511-512.
236. Sato, S., R. Nakamura, and S. Abe, *Visible-light sensitization of TiO₂ photocatalysts by wet-method N doping*. Applied Catalysis A: General, 2005. **284**(1-2): p. 131-137.
237. Xing, M., J. Zhang, and F. Chen, *New approaches to prepare nitrogen-doped TiO₂ photocatalysts and study on their photocatalytic activities in visible light*. Applied Catalysis B: Environmental, 2009. **89**(3-4): p. 563-569.
238. Cong, Y., et al., *Synthesis and characterization of nitrogen-doped TiO₂ nanophotocatalyst with high visible light activity*. The Journal of Physical Chemistry C, 2007. **111**(19): p. 6976-6982.
239. Onda, K., B. Li, and H. Petek, *Two-photon photoemission spectroscopy of Ti O 2 (110) surfaces modified by defects and O 2 or H 2 O adsorbates*. Physical Review B, 2004. **70**(4): p. 045415.
240. Pang, C.L., R. Lindsay, and G. Thornton, *Structure of clean and adsorbate-covered single-crystal rutile TiO₂ surfaces*. Chemical reviews, 2013. **113**(6): p. 3887-3948.
241. Jinlong, L., et al., *Fabrication of nitrogen-doped mesoporous TiO₂ layer with higher visible photocatalytic activity by plasma-based ion implantation*. Thin Solid Films, 2010. **519**(1): p. 101-105.
242. Premkumar, J., *Development of super-hydrophilicity on nitrogen-doped TiO₂ thin film surface by photoelectrochemical method under visible light*. Chemistry of Materials, 2004. **16**(21): p. 3980-3981.
243. Martínez-Ferrero, E., et al., *Nanostructured titanium oxynitride porous thin films as efficient visible-active photocatalysts*. Advanced Functional Materials, 2007. **17**(16): p. 3348-3354.

244. Abadias, G., et al., *Structure and properties of nitrogen-doped titanium dioxide thin films produced by reactive magnetron sputtering*. *Surface and Interface Analysis*, 2010. **42**(6-7): p. 970-973.
245. Pore, V., et al., *Atomic layer deposition of TiO₂- xNx thin films for photocatalytic applications*. *Journal of Photochemistry and Photobiology A: Chemistry*, 2006. **177**(1): p. 68-75.
246. Kafizas, A., C. Crick, and I.P. Parkin, *The combinatorial atmospheric pressure chemical vapour deposition (cAPCVD) of a grading substitutional/interstitial N-doped anatase TiO₂ thin-film; UVA and visible light photocatalytic activities*. *Journal of Photochemistry and Photobiology A: Chemistry*, 2010. **216**(2-3): p. 156-166.
247. Dunnill, C.W., et al., *Enhanced photocatalytic activity under visible light in N-doped TiO₂ thin films produced by APCVD preparations using t-butylamine as a nitrogen source and their potential for antibacterial films*. *Journal of Photochemistry and Photobiology A: Chemistry*, 2009. **207**(2-3): p. 244-253.
248. Zhao, L., Q. Jiang, and J. Lian, *Visible-light photocatalytic activity of nitrogen-doped TiO₂ thin film prepared by pulsed laser deposition*. *Applied Surface Science*, 2008. **254**(15): p. 4620-4625.
249. Mitoraj, D. and H. Kisch, *On the mechanism of urea-induced titania modification*. *Chemistry—A European Journal*, 2010. **16**(1): p. 261-269.
250. Jagadale, T.C., et al., *N-doped TiO₂ nanoparticle based visible light photocatalyst by modified peroxide sol-gel method*. *The journal of physical chemistry C*, 2008. **112**(37): p. 14595-14602.
251. Bolver, C., et al., *Nitrogen-containing TiO₂ photocatalysts: Part 1. Synthesis and solid characterization*. *Applied Catalysis B: Environmental*, 2006. **65**(3-4): p. 301-308.
252. Choi, H., et al., *Mesoporous nitrogen-doped TiO₂ for the photocatalytic destruction of the cyanobacterial toxin microcystin-LR under visible light irradiation*. *Environmental science & technology*, 2007. **41**(21): p. 7530-7535.
253. Choi, H., A.C. Sofranko, and D.D. Dionysiou, *Nanocrystalline TiO₂ photocatalytic membranes with a hierarchical mesoporous multilayer structure: synthesis, characterization, and multifunction*. *Advanced Functional Materials*, 2006. **16**(8): p. 1067-1074.
254. Choi, H., E. Stathatos, and D.D. Dionysiou, *Sol-gel preparation of mesoporous photocatalytic TiO₂ films and TiO₂/Al₂O₃ composite membranes for environmental applications*. *Applied Catalysis B: Environmental*, 2006. **63**(1-2): p. 60-67.
255. Etacheri, V., et al., *Highly visible light active TiO₂- x N x heterojunction photocatalysts*. *Chemistry of Materials*, 2010. **22**(13): p. 3843-3853.
256. Zhu, X., et al., *Photocatalytic formaldehyde oxidation over plasmonic Au/TiO₂ under visible light: moisture indispensability and light enhancement*. *ACS Catalysis*, 2017. **7**(10): p. 6514-6524.

257. Hirai, K., S. Isobe, and K. Sada, *Gas-generated thermal oxidation of a coordination cluster for an anion-doped mesoporous metal oxide*. Scientific reports, 2015. **5**(1): p. 1-9.
258. Nagaveni, K., et al., *Synthesis and structure of nanocrystalline TiO₂ with lower band gap showing high photocatalytic activity*. Langmuir, 2004. **20**(7): p. 2900-2907.
259. Kamisaka, H., T. Adachi, and K. Yamashita, *Theoretical study of the structure and optical properties of carbon-doped rutile and anatase titanium oxides*. The Journal of chemical physics, 2005. **123**(8): p. 084704.
260. Xia, T., et al., *A facile method to improve the photocatalytic and lithium-ion rechargeable battery performance of TiO₂ nanocrystals*. Advanced Energy Materials, 2013. **3**(11): p. 1516-1523.
261. Lin, X., et al., *Carbon-doped mesoporous TiO₂ film and its photocatalytic activity*. Microporous and Mesoporous Materials, 2011. **142**(1): p. 276-281.
262. Fattori, A., et al., *Fast hole surface conduction observed for indoline sensitizer dyes immobilized at fluorine-doped tin oxide– TiO₂ surfaces*. The Journal of Physical Chemistry C, 2010. **114**(27): p. 11822-11828.
263. Shifu, C., Y. Yunguang, and L. Wei, *Preparation, characterization and activity evaluation of TiN/F-TiO₂ photocatalyst*. Journal of hazardous materials, 2011. **186**(2-3): p. 1560-1567.
264. Xing, M., et al., *Super-hydrophobic fluorination mesoporous MCF/TiO₂ composite as a high-performance photocatalyst*. Journal of catalysis, 2012. **294**: p. 37-46.
265. Cui, Y., H. Du, and L.S. Wen. *Investigation of Electronic Structures of F-doped TiO₂ by First-principles Calculation*. in *Materials Science Forum*. 2009. Trans Tech Publ.
266. Bashir, A., Inayat, A., Bashir, R., Abbas, S. M., Sultan, M., Iqbal, A., & Akhter, Z. (2023). Design of Porous Ni and Rare Earth Metals (Ce, Ho, and Eu) Co-doped TiO₂ Nanoarchitectures for Energy Conversion and Storage Applications. *New Journal of Chemistry*.
267. Gonzalez-Hernandez, R., et al., *Study of the properties of undoped and fluorine doped zinc oxide nanoparticles*. Materials Letters, 2010. **64**(13): p. 1493-1495.
268. Periyat, P., et al., *One-pot synthesis of anionic (nitrogen) and cationic (sulfur) codoped high-temperature stable, visible light active, anatase photocatalysts*. The Journal of Physical Chemistry C, 2009. **113**(8): p. 3246-3253.
269. Periyat, P., et al., *Improved high-temperature stability and sun-light-driven photocatalytic activity of sulfur-doped anatase TiO₂*. The Journal of Physical Chemistry C, 2008. **112**(20): p. 7644-7652.
270. Han, C., et al., *Innovative visible light-activated sulfur doped TiO₂ films for water treatment*. Applied Catalysis B: Environmental, 2011. **107**(1-2): p. 77-87.
271. Seo, H., et al., *Generation of highly n-type titanium oxide using plasma fluorine insertion*. Nano letters, 2011. **11**(2): p. 751-756.

272. Zhao, W., et al., *Efficient degradation of toxic organic pollutants with Ni₂O₃/TiO_{2-x}B_x under visible irradiation*. Journal of the American Chemical Society, 2004. **126**(15): p. 4782-4783.
273. Quesada-González, M., et al., *Interstitial boron-doped TiO₂ thin films: the significant effect of boron on TiO₂ coatings grown by atmospheric pressure chemical vapor deposition*. ACS applied materials & interfaces, 2016. **8**(38): p. 25024-25029.
274. Stengl, V., et al., *Photocatalytic activity of boron-modified titania under UV and visible-light illumination*. ACS Applied Materials & Interfaces, 2010. **2**(2): p. 575-580.
275. Xing, M.-Y., et al., *Formation of new structures and their synergistic effects in boron and nitrogen codoped TiO₂ for enhancement of photocatalytic performance*. The Journal of Physical Chemistry C, 2011. **115**(16): p. 7858-7865.
276. Czoska, A., et al., *The nitrogen–boron paramagnetic center in visible light sensitized N–B co-doped TiO₂. Experimental and theoretical characterization*. Physical Chemistry Chemical Physics, 2011. **13**(1): p. 136-143.
277. Nasr, M., et al., *High photodegradation and antibacterial activity of BN–Ag/TiO₂ composite nanofibers under visible light*. New Journal of Chemistry, 2018. **42**(2): p. 1250-1259.
278. Yang, Y. and C. Tian, *Effects of Calcining Temperature on Photocatalytic Activity of Fe-Doped Sulfated Titania*. Photochemistry and photobiology, 2012. **88**(4): p. 816-823.
279. Liu, H., Y. Wu, and J. Zhang, *A new approach toward carbon-modified vanadium-doped titanium dioxide photocatalysts*. ACS applied materials & interfaces, 2011. **3**(5): p. 1757-1764.
280. Wang, W., et al., *Preparation and characterization of visible-light-driven N–F–Ta tri-doped TiO₂ photocatalysts*. Applied surface science, 2012. **258**(22): p. 8696-8703.
281. Cong, Y., et al., *Carbon and nitrogen-codoped TiO₂ with high visible light photocatalytic activity*. Chemistry Letters, 2006. **35**(7): p. 800-801.
282. Liu, G., et al., *Synergistic effects of B/N doping on the visible-light photocatalytic activity of mesoporous TiO₂*. Angewandte Chemie International Edition, 2008. **47**(24): p. 4516-4520.
283. In, S., et al., *Effective visible light-activated B-doped and B, N-codoped TiO₂ photocatalysts*. Journal of the American Chemical Society, 2007. **129**(45): p. 13790-13791.
284. Singh, B., et al., *Nanostructured BN–TiO₂ composite with ultra-high photocatalytic activity*. New Journal of Chemistry, 2017. **41**(20): p. 11640-11646.
285. Komai, Y., et al., *Visible light response of nitrogen and sulfur co-doped TiO₂ photocatalysts fabricated by anodic oxidation*. Catalysis today, 2011. **164**(1): p. 399-403.
286. Yang, G., et al., *Low-Temperature Synthesis of Visible-Light Active Fluorine/Sulfur Co-doped Mesoporous TiO₂ Microspheres*. Chemistry–A European Journal, 2011. **17**(4): p. 1096-1100.

287. Wu, Y., et al., *Preparation of nitrogen and fluorine co-doped mesoporous TiO₂ microsphere and photodegradation of acid orange 7 under visible light*. Chemical Engineering Journal, 2010. **162**(2): p. 710-717.
288. Wu, Y., M. Xing, and J. Zhang, *Gel-hydrothermal synthesis of carbon and boron co-doped TiO₂ and evaluating its photocatalytic activity*. Journal of hazardous materials, 2011. **192**(1): p. 368-373.
289. Wei, H., et al., *Preparation and photocatalysis of TiO₂ nanoparticles co-doped with nitrogen and lanthanum*. Journal of materials science, 2004. **39**(4): p. 1305-1308.
290. Biswas, A., A. Chakraborty, and N.R. Jana, *Nitrogen and fluorine codoped, colloidal TiO₂ nanoparticle: tunable doping, large red-shifted band edge, visible light induced photocatalysis, and cell death*. ACS applied materials & interfaces, 2017. **10**(2): p. 1976-1986.
291. Cong, Y., et al., *Preparation, photocatalytic activity, and mechanism of nano-TiO₂ co-doped with nitrogen and iron (III)*. The Journal of Physical Chemistry C, 2007. **111**(28): p. 10618-10623.
292. Wong, M.-S., et al., *Antibacterial property of Ag nanoparticle-impregnated N-doped titania films under visible light*. Scientific reports, 2015. **5**(1): p. 1-11.
293. Hoang, S., et al., *Enhancing visible light photo-oxidation of water with TiO₂ nanowire arrays via cotreatment with H₂ and NH₃: synergistic effects between Ti³⁺ and N*. Journal of the American Chemical Society, 2012. **134**(8): p. 3659-3662.
294. Dhandole, L.K., et al., *Enhanced photocatalytic degradation of organic pollutants and inactivation of *Listeria monocytogenes* by visible light active Rh-Sb codoped TiO₂ nanorods*. ACS Sustainable Chemistry & Engineering, 2018. **6**(3): p. 4302-4315.
295. Etacheri, V., et al., *Oxygen rich titania: A dopant free, high temperature stable, and visible-light active anatase photocatalyst*. Advanced Functional Materials, 2011. **21**(19): p. 3744-3752.
296. Assadi, A.A., A. Bouzaza, and D. Wolbert, *Photocatalytic oxidation of trimethylamine and isovaleraldehyde in an annular reactor: influence of the mass transfer and the relative humidity*. Journal of photochemistry and photobiology A: Chemistry, 2012. **236**: p. 61-69.
297. Verbruggen, S.W., S. Lenaerts, and S. Denys, *Analytic versus CFD approach for kinetic modeling of gas phase photocatalysis*. Chemical Engineering Journal, 2015. **262**: p. 1-8.
298. Lopes, F.V., et al., *Insights into UV-TiO₂ photocatalytic degradation of PCE for air decontamination systems*. Chemical engineering journal, 2012. **204**: p. 244-257.
299. Monteiro, R.A., et al., *Are TiO₂-based exterior paints useful catalysts for gas-phase photooxidation processes? A case study on n-decane abatement for air detoxification*. Applied Catalysis B: Environmental, 2014. **147**: p. 988-999.
300. Lopes, F.V., et al., *Perchloroethylene gas-phase degradation over titania-coated transparent monoliths*. Applied Catalysis B: Environmental, 2013. **140**: p. 444-456.

301. Sacco, O., V. Vaiano, and D. Sannino, *Main parameters influencing the design of photocatalytic reactors for wastewater treatment: a mini review*. Journal of Chemical Technology & Biotechnology, 2020. **95**(10): p. 2608-2618.
302. Chong, S., et al., *Simulations of photodegradation of toluene and formaldehyde in a monolith reactor using computational fluid dynamics*. AIChE journal, 2011. **57**(3): p. 724-734.
303. Obee, T.N., *Photooxidation of sub-parts-per-million toluene and formaldehyde levels on titania using a glass-plate reactor*. Environmental Science & Technology, 1996. **30**(12): p. 3578-3584.
304. Passalía, C., et al., *Photocatalytic degradation of formaldehyde in gas phase on TiO₂ films: a kinetic study*. International Journal of Chemical Reactor Engineering, 2010. **8**(1).
305. Passalía, C., O.M. Alfano, and R.J. Brandi, *Optimal design of a corrugated-wall photocatalytic reactor using efficiencies in series and computational fluid dynamics (CFD) modeling*. Industrial & Engineering Chemistry Research, 2013. **52**(21): p. 6916-6922.
306. Assadi, A.A., et al., *Abatement of 3-methylbutanal and trimethylamine with combined plasma and photocatalysis in a continuous planar reactor*. Journal of Photochemistry and Photobiology A: Chemistry, 2014. **282**: p. 1-8.
307. Passalía, C., O.M. Alfano, and R.J. Brandi, *Modeling and experimental verification of a corrugated plate photocatalytic reactor using computational fluid dynamics*. Industrial & engineering chemistry research, 2011. **50**(15): p. 9077-9086.
308. Imoberdorf, G.E., et al., *Scaling-up from first principles of a photocatalytic reactor for air pollution remediation*. Chemical engineering science, 2007. **62**(3): p. 793-804.
309. Imoberdorf, G.E., et al., *Photocatalytic degradation of tetrachloroethylene in gas phase on TiO₂ films: A kinetic study*. Industrial & engineering chemistry research, 2005. **44**(16): p. 6075-6085.
310. Demeestere, K., et al., *A new kinetic model for titanium dioxide mediated heterogeneous photocatalytic degradation of trichloroethylene in gas-phase*. Applied Catalysis B: Environmental, 2004. **54**(4): p. 261-274.
311. Muñoz-Batista, M.J., et al., *Sunlight-driven toluene photo-elimination using CeO₂-TiO₂ composite systems: A kinetic study*. Applied Catalysis B: Environmental, 2013. **140**: p. 626-635.
312. Geng, Q., Q. Guo, and X. Yue, *Adsorption and photocatalytic degradation kinetics of gaseous cyclohexane in an annular fluidized bed photocatalytic reactor*. Industrial & engineering chemistry research, 2010. **49**(10): p. 4644-4652.
313. Shan, A.Y., T.I.M. Ghazi, and S.A. Rashid, *Immobilisation of titanium dioxide onto supporting materials in heterogeneous photocatalysis: a review*. Applied Catalysis A: General, 2010. **389**(1-2): p. 1-8.
314. Krajewski, J.J., *Non-destructive depth profiling using variable kinetic energy-x-ray photoelectron spectroscopy with maximum entropy regularization*. 2016: University of Delaware.

315. Nizard, H., et al., *Deposition of titanium dioxide from TTIP by plasma enhanced and remote plasma enhanced chemical vapor deposition*. Surface and Coatings Technology, 2008. **202**(17): p. 4076-4085.
316. Sun, H., et al., *Photocatalytic TiO₂ films prepared by chemical vapor deposition at atmosphere pressure*. Journal of Non-Crystalline Solids, 2008. **354**(12-13): p. 1440-1443.
317. Lopez, L., et al., *Effect of substrate on surface morphology and photocatalysis of large-scale TiO₂ films*. Applied Surface Science, 2013. **265**: p. 162-168.
318. Sampaio, M.J., et al., *Photocatalytic activity of TiO₂-coated glass raschig rings on the degradation of phenolic derivatives under simulated solar light irradiation*. Chemical engineering journal, 2013. **224**: p. 32-38.
319. Kete, M., et al., *Highly active photocatalytic coatings prepared by a low-temperature method*. Environmental Science and Pollution Research, 2014. **21**(19): p. 11238-11249.
320. Tennakone, K., C. Tilakaratne, and I. Kottegoda, *Photocatalytic degradation of organic contaminants in water with TiO₂ supported on polythene films*. Journal of Photochemistry and Photobiology A: Chemistry, 1995. **87**(2): p. 177-179.
321. Yu, J.C., et al., *Influence of thermal treatment on the adsorption of oxygen and photocatalytic activity of TiO₂*. Langmuir, 2000. **16**(18): p. 7304-7308.
322. Robert, D., V. Keller, and N. Keller, *Immobilization of a semiconductor photocatalyst on solid supports: methods, materials, and applications*. Photocatalysis and water purification: from fundamentals to recent applications, 2013: p. 145-178.
323. Priya, D.N., J.M. Modak, and A.M. Raichur, *LbL fabricated poly (styrene sulfonate)/TiO₂ multilayer thin films for environmental applications*. ACS applied materials & interfaces, 2009. **1**(11): p. 2684-2693.
324. Krogman, K.C., et al., *Photocatalytic layer-by-layer coatings for degradation of acutely toxic agents*. Chemistry of Materials, 2008. **20**(5): p. 1924-1930.
325. Nakajima, A., et al., *Preparation and properties of Cu-grafted transparent TiO₂-nanosheet thin films*. Materials Letters, 2009. **63**(20): p. 1699-1701.
326. Bavykin, D.V., L. Passoni, and F.C. Walsh, *Hierarchical tube-in-tube structures prepared by electrophoretic deposition of nanostructured titanates into a TiO₂ nanotube array*. Chemical Communications, 2013. **49**(62): p. 7007-7009.
327. Raddaha, N.S., et al., *Electrophoretic deposition of chitosan/h-BN and chitosan/h-BN/TiO₂ composite coatings on stainless steel (316L) substrates*. Materials, 2014. **7**(3): p. 1814-1829.
328. Chen, H.-W., et al., *Electrophoretic deposition of mesoporous TiO₂ nanoparticles consisting of primary anatase nanocrystallites on a plastic substrate for flexible dye-sensitized solar cells*. Chemical Communications, 2011. **47**(29): p. 8346-8348.
329. Chávez-Valdez, A., M. Herrmann, and A. Boccaccini, *Alternating current electrophoretic deposition (EPD) of TiO₂ nanoparticles in aqueous suspensions*. Journal of colloid and interface science, 2012. **375**(1): p. 102-105.

330. Sakthivel, S. and H. Kisch, *Daylight photocatalysis by carbon-modified titanium dioxide*. *Angewandte Chemie International Edition*, 2003. **42**(40): p. 4908-4911.
331. Morikawa, T., et al., *Band-gap narrowing of titanium dioxide by nitrogen doping*. *Japanese Journal of Applied Physics*, 2001. **40**(6A): p. L561.